POLITECNICO DI TORINO

Collegio di Ingegneria Civile

**Corso di Laurea Magistrale
in Ingegneria Civile**

Tesi di Laurea Magistrale

Investigating linear and non-linear damage behaviour of bituminous binders by means of continuum damage approach

Relatore

prof. Santagata, Ezio

Correlatori

prof. Baglieri, Orazio
prof. Riviera, Pier
prof.ssa Tsantilis, Lucia

Candidato

Juan Pablo Reginatto

Marzo 2018

Table of Contents

Introduction

Fatigue is one of the main distresses of asphalt concrete mixtures. This phenomenon is mostly influenced by the behaviour of the asphalt binder due to the fact that damage takes place mainly on this component.

One of the most important consequences of damage is the appearance of microcracks that turn into macrocracks as the loading process persists.

From another perspective, damage also appears as a nonlinearity. In other words, it's partly responsible for the decrease of the complex modulus under certain loading conditions.

Another nonlinearity that must be taken into account on the study of the material is the NLVE (nonlinear viscoelastic) behavior.

The differentiation or isolation of the different nonlinearities is a key part of the bitumen characterization.

An effective way of describing the fatigue response of a material is the $C - S$ curve, which traces how the pseudo secant modulus (C) decreases as damage increases. Damage is quantified by an internal state variable called S. This procedure is a part of the VECD (viscoelastic continuum damage) model which will be thoroughly described on the next chapter.

The VECD model takes advantage of the viscoelastic correspondence principle. It allows to replace certain variables with pseudo variables in order to remove the viscoelastic effects from the analysis, in other words, to perform an elastic analysis of a viscoelastic problem.

On the following chapters an analysis of four different binders is presented. Feyzin, Mantova, PG-64-22 and PG-76-16. The tests were performed over the original binders and in some cases over the PAV binders.

The first part of the study is about the linear characterization of the materials. The tests performed on this section aimed to determine the linear range (on which the behavior isn't strain dependent), also to obtain the master curves and the Prony series representation of the relaxation modulus E(t) and creep compliance D(t).

After the linear analysis, several tests were performed in order to comprehend the behavior of the binders outside the linear range. Outward this range, a decrease on the complex modulus can be observed as the strain applied to the material is increased.

This tests have allowed to develop a model that characterize the strain dependent nature of the material.

The final set of tests consisted on submitting the binders to different levels of strains with a sinusoidal load. The final goal of the test is to realize how the reduction of the modulus takes place. This reduction is caused by fatigue.

Due to the viscoelastic nature of asphalt binders, all tests are performed taking into account the dependency of the behavior regarding temperature, frequency of loading and time.

In all cases, the tests were performed with a rheometer. This device measures the strains and shear stresses that a binder sample undergoes when it's submitted to torque.

The first chapter of this work is about the theoretical background on which the tests are based. The second chapter is about the experimental program, that is to say, materials, instruments, test procedures, etc.

Finally, the third chapter is dedicated to the results analysis.

Chapter 1: Theoretical Background

1.1 Linear viscoelastic behavior

1.1.1 General concept

Unlike elastic materials, the behavior of viscoelastic materials is dependent on temperature and time. That means that the loading history of the material must be known in order to predict its current state.
Having a linear behavior means that strains are completely recoverable.
The constitutive relationships of these kind of materials can be represented by convolution integrals, as shown in equation 1 and 2 (Underwood, 2006).

$$\sigma = \int_0^t E(t - \tau) \cdot \frac{d\varepsilon}{d\tau} \cdot d\tau \tag{1}$$

$$\varepsilon = \int_0^t D(t - \tau) \cdot \frac{d\sigma}{d\tau} \cdot d\tau \tag{2}$$

Where, E(t) is the relaxation modulus, $D(t)$ the creep compliance (section 1.1.2) and τ an integration variable.

1.1.2 Creep and Relaxation

The phenomenon of creep occurs when a material suffers a slow continuous deformation under constant stress. For linear materials, strain can be obtained with eq. 3.

$$\varepsilon(t) = \sigma_0 \cdot D(t) \tag{3}$$

Where, σ_0 is the applied constant stress and $D(t)$ the creep compliance.
On the other hand, relaxation occurs when a material is subjected to permanent deformation. In this case, stress gradually decreases. For linear materials, the stress can be represented by eq. 4.

$$\sigma(t) = \varepsilon_0 \cdot E(t) \tag{4}$$

Where, ε_0 is the applied permanent strain and $E(t)$ the relaxation modulus.
The creep compliance function and the relaxation modulus function depend on the material properties (Findley, et al., 1976).

1.1.3 Complex modulus

The complex modulus $E^*(t)$ is a constitutive relationship between the deformation and a steady sinusoidal loading. It's divided into two components, the storage modulus $E'(t)$ (eq. 5) and the loss modulus $E''(t)$ (eq. 6).

$$E'(t) = E^*(t) \cdot \cos(\delta(w_R)) \tag{5}$$

$$E''(t) = E^*(t) \cdot sen(\delta(w_R)) \qquad (6)$$

$$E^*(t) = E'(t) + i \cdot E''(t) \qquad (7)$$

Where, δ is the phase angle and w_R the reduced frequency.
In purely elastic materials, the phase angle equals 0°. This means that deformation response occurs simultaneously with load (stress and strain in phase). On the other hand, purely viscous materials have a 90° phase angle.

1.1.4 Time-temperature correspondence principle

Linear viscoelastic behavior has a time – frequency correlation. In fact, a certain material subjected to low frequencies and high temperatures can have the same response that it would have at high frequencies and low temperatures. This principle is very useful due to the fact that it allows to perform tests in a limited range of frequencies and temperatures and it's still possible to know the material's behavior outside this range.
The parameter that takes into account both variables is the reduced frequency w_R (eq. 8).

$$w_R = w \cdot a(T) \qquad (8)$$

Where, w is the frequency and $a(T)$ the shift factor.
The shift factor is a temperature dependent function that moves horizontally the Complex Modulus Vs Frequency curves obtained at different temperatures in order to create a single curve called master curve which describes the constitutive behavior of binders. This process can be observed on fig.1.
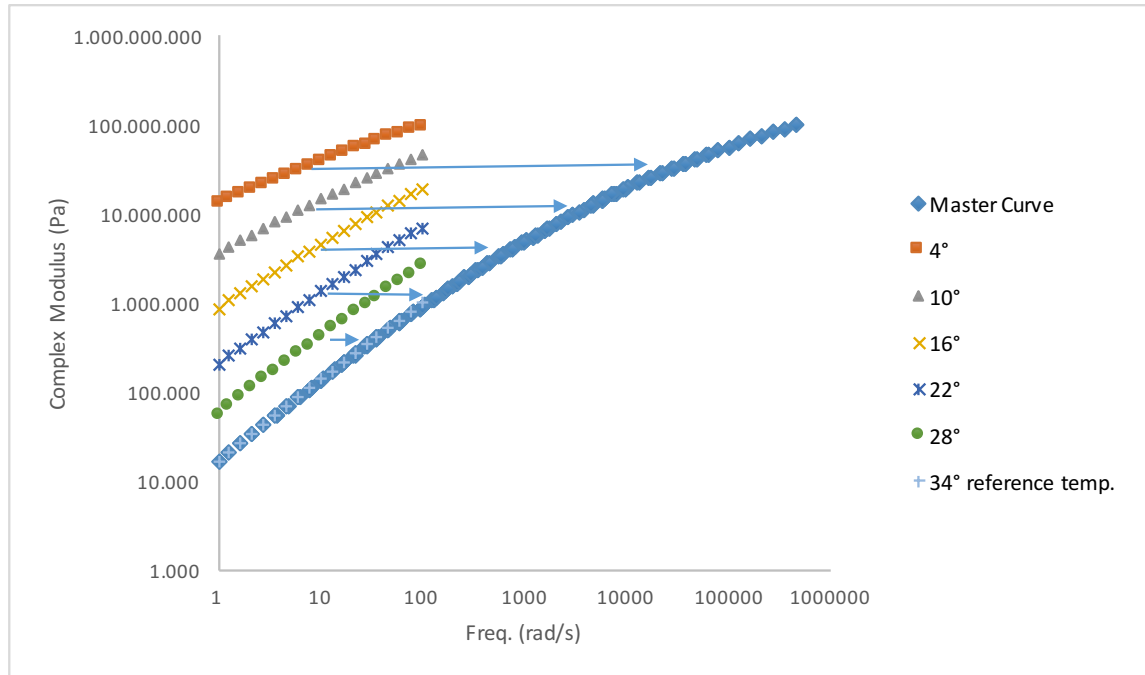

Fig. 1. Master curve
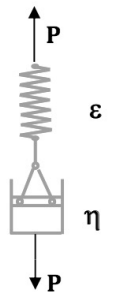
1.2 Viscoelastic Models

In the following section, viscoelastic models are presented. These are used for the study of the stress – strain – time relationships.
Mechanical models are used for the representation of the behavior when the applied load is steady. They are made up of dashpots and springs. The best describing model depends on the type of bitumen and temperature.
On the other hand, for oscillating loading regimes, analytical models are used.

1.2.1 Maxwell model

This model consists in one spring and one dashpot connected in series (fig 2). Therefore, the total strain is the summation of the spring strain and the dashpot strain (eq. 9).

$$\varepsilon = \varepsilon_{spring} + \varepsilon_{dashpot} \tag{9}$$

$$\left(\frac{d\varepsilon}{dt}\right) = \frac{1}{E} \cdot \frac{d\sigma}{dt} + \frac{\sigma}{\eta} \tag{10}$$

$$\varepsilon(t) = \left(\frac{1}{E} + \frac{t}{\eta}\right) \cdot \sigma \tag{11}$$
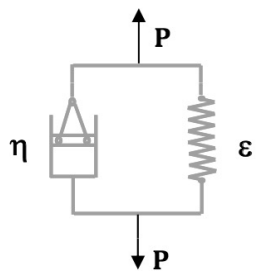
Fig. 2

Where, η is the coefficient of viscosity.
This model describes a liquid – like behavior.

1.2.2 Kelvin Voigt Model

This model consists in one spring and one dashpot connected in parallel (fig. 3). Therefore, the total stress is the summation of the spring stress and the dashpot stress (eq. 12).

$$\sigma = \sigma_{spring} + \sigma_{dashpot} \tag{12}$$

$$\sigma = E \cdot \varepsilon + \eta \cdot \frac{d\varepsilon}{dt} \tag{13}$$

$$\varepsilon(t) = \varepsilon_0 \cdot \left[1 - e^{\left(-\frac{t}{\lambda}\right)}\right] \tag{14}$$

Fig. 3

Where, $\lambda = \eta/E$ is the relaxation time.
This model describes a solid – like behavior.

1.2.3 Burger Model

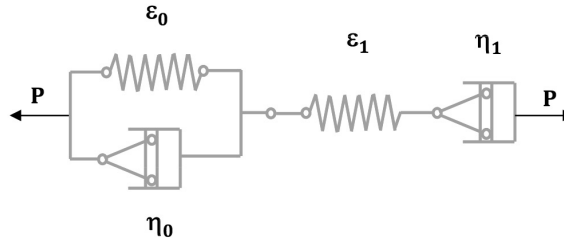This model consists in a Maxwell model connected in series with a Kelvin Voight model (fig. 4).

Fig. 4

$$\varepsilon(t) = \frac{\sigma}{E_0} + \frac{\sigma}{\eta_0} \cdot (t - t_0) + \frac{\sigma}{E_1} \cdot \left[e^{\left(-\frac{t-t_0}{\lambda_1}\right)} \right] \tag{15}$$

The Burger model describes a behavior between a solid and a liquid like behavior

1.2.4 Prony series representation

The Prony series describes the behavior of a Maxwell model subjected to oscillating loading. The storage modulus, the loss modulus and the relaxation modulus can be expressed as a time dependent property by means of the Prony series (Yun, et al., 2010), as shown in eq. 16, 17 and 18.

$$G'(w_R) = \sum_{m=1}^{n} \frac{w_R^2 \cdot \rho_m^2 \cdot G_m}{w_R^2 \cdot \rho_m^2 + 1} \tag{16}$$

$$G''(w_R) = \sum_{m=1}^{n} \frac{w_R \cdot \rho_m \cdot G_m}{w_R^2 \cdot \rho_m^2 + 1} \tag{17}$$

$$G(t) = \sum_{m=1}^{n} G_m \cdot e^{\frac{-t}{\rho_m}} \tag{18}$$

Where, $G'(w_R)$ = storage modulus; $G''(w_R)$ = loss modulus; w_R = reduced angular freq.; G_m = modulus of one of Maxwell elements; ρ_i = relaxation time.
If the loading frequency equals infinity, the dynamic modulus equals the spring constant of the Maxwell model (Findley, et al., 1976).

1.2.5 Christensen - Anderson – Marasteanu model (CAM model)

One way of approximately describing the master curve is by means of the CAM Model. It's an analytic model that provides formulation for the modelling of not only the master curve (eq. 19) but also the phase angle curve (eq. 20) (Marasteanu & Anderson, 1999).

$$G^*(w_R) = G_g \cdot \left[1 + \left(\frac{w_c}{w_R} \right)^{\frac{\log(2)}{R}} \right]^{-\frac{R \cdot m}{\log(2)}} \tag{19}$$

$$\delta(w_R) = \frac{90 \cdot m}{\left[1 + \left(\frac{w_R}{w_c}\right)^{\frac{\log(2)}{R}}\right]} \tag{20}$$

Where, $G^*(w_R)$ = complex modulus; $\delta(w_R)$ = phase angle; G_g = the glassy modulus; R = rheological index; w_c = cross over frequency; and m = model parameter.

1.2.6 Nonlinear viscoelastic shift factors

Outside the linear range, nonlinearities appear. The behavior becomes strain dependent. The nonlinear viscoelastic behavior can be modelled by means of two shift factors, a_γ and h_1. Both are functions of the strain and their influence can be observed in eq. 21 and eq. 22 (Underwood, 2015)

$$w_r' = w_r \cdot a_\gamma = (a_T \cdot w) \cdot a_\gamma \tag{21}$$

Where, w_r' is the strain dependent reduced frequency and w_r the reduced frequency.

$$\tau(w_r) = h_1 \cdot G^*(w_r')[\gamma_e(w_r)] \tag{22}$$

Where, γ_e is the effective strain.

$$t_r' = \frac{t}{a_T \cdot a_\gamma} \tag{23}$$

Where, t_r' is the strain dependent reduced time.
In the case of the Prony series representation the influence of a_γ and h_1 can be seen in eq. 24.

$$G_{NLVE}' = h_1 \cdot \sum \frac{G_m \cdot (w_R \cdot a_\gamma)^2 \cdot \rho_m^2}{\rho_m^2 \cdot (w_R \cdot a_\gamma)^2 + 1} \tag{24}$$

Where, G_{NLVE}' = nonlinear storage modulus; w_R = reduced angular frequency; G_i = modulus of one of Maxwell elements; ρ_i = relaxation time.

1.3 Viscoelastic Continuum Damage Model

The VCDM is based on three main concepts: the elastic – viscoelastic correspondence principle, Schapery's work potential theory and the time – temperature correspondence principle (Hou, et al., 2010).

1.3.1 Elastic – viscoelastic correspondence principle

This principle was introduced by Schapery (Schapery, 1984). He proposed that viscoelastic problems can be treated as elastic problems using elastic constitutive equations and by

considering stresses and strains as pseudo variables. On eq. 25, the convolution integral of the pseudo strain.

$$\gamma^R = \frac{1}{G_R} \cdot \int_0^t G(t - \tau) \cdot \frac{d\gamma}{d\tau} \cdot d\tau \qquad (25)$$

Where, $G(t)$ is the relaxation modulus, G_R the reference modulus and γ the real strain.
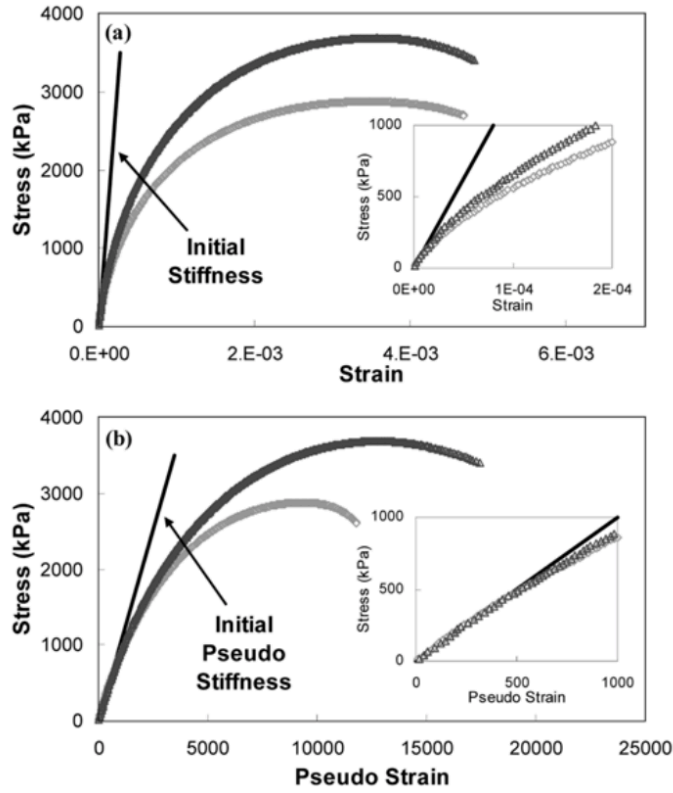
Fig. 5. (Kim, et al., 2008)

On fig. 5. (Kim, et al., 2008) picture (a) there's a stress strain space. On picture (b) there's a stress pseudo strain space. On picture (a) the nonlinear behavior starts from the beginning of the curve due to mainly time effects. On the other hand, on picture (b) the nonlinear behavior starts after. On this case the nonlinearity is only due to damage.

Therefore, working with pseudo strain allows to remove from the analysis the nonlinear effects caused by time.

A simplification is introduced in order to facilitate calculations (Underwood, 2015). This simplification assumes a steady – state condition so instead of eq. 25, eq. 26 is used for the calculation of the pseudo strain.

$$(\gamma_{pp}^R) = \frac{h_1}{G_R} \cdot \left[(\gamma_{0,pp}) \right] \cdot |G^*|(w_r') \qquad (26)$$

Where, $\gamma_{0,pp}$ is the peak to peak strain.

In the stress – pseudo strain space the way of quantifying the effective stiffness is by means of the instantaneous secant modulus (eq. 27).

$$C = \frac{\tau}{\gamma^R \cdot DMR} \tag{27}$$

Where, DMR is the dynamic modulus ratio (eq. 28). It's used to normalize the tests for specimen to specimen variability (Underwood, 2012).

$$DMR = \frac{|G^*|_{fingerprint}}{|G|_{LVE}} \tag{28}$$

Where, $|G^*|_{fingerprint}$ is the complex modulus at small strains, therefore without damage.

1.3.2 Schapery's work potential theory

This theory is based on thermodynamic principles. It was developed by Schapery to characterize how damage grows in elastic materials (Schapery, 1990).
The WPT is based on three main functions, the pseudo strain energy density function (eq. 29), the stress – pseudo strain relationship (eq. 30) and the damage evolution law (eq. 31) (Zeiada, et al., 2014).

$$W^R = f(\varepsilon^R, S) = \frac{1}{2} \cdot C(S) \cdot (\gamma^R)^2 \tag{29}$$

$$\sigma = \frac{\partial W^R}{\partial \varepsilon^R} \tag{30}$$

$$\frac{dS}{dt} = \left(-\frac{\partial W^R}{\partial S} \right)^\alpha \tag{31}$$

Where, S is an internal state variable that quantifies damage by taking into account microstructural changes that lead to a reduction of stiffness and α is the damage evolution rate. α is introduced to take into account a time dependency that's not included on the pseudo strain analysis due to the fact that it's related to damage growth. It can be calculated with the steady state log – log slope of the mastercurve (m) (eq. 32) (Underwood, 2015).

$$\alpha = \frac{1}{m} + 1 \tag{32}$$

If eq. 29 is substituted into eq. 31, eq. 33 is obtained. It's important to note that only the pseudo stiffness (C) is function of damage (S).

$$\frac{dS}{dt'_r} = \left(-\frac{1}{2} \cdot (\gamma^R)^2 \cdot \frac{dC}{dS} \right)^\alpha \tag{33}$$

Underwood introduces a simplification to solve eq. 33 (Underwood, 2015):
Eq. 34 allows to calculate damage occurring on a load cycle.

$$\Delta S = \int_{t'_{r,initial}}^{t'_{r,final}} \left(-\frac{1}{2} \cdot (\gamma^R)^2 \cdot \frac{dC}{dS} \right)^{\alpha} dt'_r \qquad (34)$$

Where, $t'_{r,final} - t'_{r,initial}$ equals the reduced period of loading (t'_{rp}) and γ^R (pseudo strain) is a function presented in eq. 35.

$$\gamma^R(t'_r) = \gamma_{pp}^R \cdot \frac{\sin(w_r \cdot t'_r)}{2} = \gamma_{pp}^R \cdot f(t'_r) \qquad (35)$$

In eq. 36 a cycle wise damage function is introduced. This function considers that steady state deformations exist. This assumption simplifies the calculations. However, this assumption is not actually true, that's why a correction factor is introduced (B_1).

$$\Delta S = \left(-\frac{1}{2} \cdot (\gamma_{pp}^R)^2 \cdot \frac{dC^*}{dS} \right)^{\alpha} \cdot \left(t'_{r,final} - t'_{r,initial} \right) \cdot B_1 \qquad (36)$$

Where, C^* is defined in eq. 37.

$$C^* = \frac{\tau_{pp}}{\gamma_{pp}^R \cdot DMR} \qquad (37)$$

Considering that the damage generated in one cycle is very small, C^* is very similar to C (Underwood, et al., 2010). Besides, according to Underwood (Underwood, 2015), we can also assume that dC/dS during one cycle is constant, therefore eq. 34 can be rewritten into eq. 38.

$$\Delta S = \left(\frac{dC}{dS} \right)^{\alpha} \cdot \left[\int_{t'_{r,initial}}^{t'_{r,final}} \left(-\frac{1}{2} \cdot (\gamma^R)^2 \right)^{\alpha} dt'_r \right] \qquad (38)$$

Setting eq. 36 equal to eq.38 and considering the assumptions explained on the previous paragraph, the B_1 correction factor is obtained (eq. 39).

$$B_1 = \frac{1}{(t'_{r,final} - t'_{r,initial})} \cdot \int_{t'_{r,initial}}^{t'_{r,final}} \left(f(t'_r) \right)^{2\alpha} dt'_r \qquad (39)$$

The steady state deformation and constant damage rate assumptions aren't valid on the first loading cycles due to the fact that during these, rapid changes on the binder state occur. Therefore, in this case the piecewise formulation must be used.
To sum up, for the calculation of C, γ^R and ΔS eq. 40 – 42 are used (Underwood, 2015)

$$C = \begin{cases} C = \dfrac{\tau}{\gamma^R \cdot DMR} & t'_r \le t'_{rp} \\[3mm] C^* = \dfrac{\tau_{pp}}{\gamma_{pp}^R \cdot DMR} & t'_r > t'_{rp} \end{cases} \qquad (40)$$

$$\gamma^R = \begin{cases} \gamma^R = \dfrac{h_1}{G_R} \displaystyle\int_0^{t'_r} G(t'_r - \xi)\dfrac{d(h_2\gamma)}{d\xi}d\xi & t'_r \leq t'_{rp} \\[4mm] (\gamma^R_{pp}) = \dfrac{h_1}{G_R} \cdot [(\gamma_{0,pp})] \cdot |G^*|(w'_r) & t'_r > t'_{rp} \end{cases} \tag{41}$$

$$\Delta S = \begin{cases} \Delta S = \left(-\dfrac{1}{2} \cdot \left(\gamma^R{}_{j+1}\right)^2 \cdot (C_{j+1} - C_j)\right)^{\frac{\alpha}{1+\alpha}} (t'^{(j+1)}_r - t'^{(j)}_r)^{\frac{1}{1+\alpha}} & t'_r \leq t'_{rp} \\[4mm] \Delta S = \left(-\dfrac{1}{2} \cdot \left(\gamma^R{}_{pp}\right)^2 \cdot (C_{i+N} - C_i)\right)^{\frac{\alpha}{1+\alpha}} (t'^{(j+1)}_{rp} \cdot N)^{\frac{1}{1+\alpha}} \cdot B_1 & t'_r > t'_{rp} \end{cases} \tag{42}$$

The formulae presented above (eq. 42) allow to know the quantity of damage (S) on each cycle. Confronting S with C (eq.40) enables the creation of the damage characteristic curve. This curve is inherent to the material and it doesn't depend on temperature, frequency of loading, strain, e.g. (Zeiada, et al., 2014)
The damage characteristic curve can be approximated with eq. 43

$$C^* = a \cdot S^3 + b \cdot S^2 + c \cdot S + d \tag{43}$$

Where, a, b, c and d are regression coefficients.

1.3.3 Time-temperature correspondence principle

It has been demonstrated that the time temperature correspondence principle is also valid in the nonlinear range of the material. (Yun, et al., 2010).
That means that the shift factors obtained in the linear analysis are still usable when the material has suffered damage and permanent strain.

Chapter 2: Experimental Program

2.1 Dynamic shear rheometer (DSR)

The DSR is a very useful device for the characterization of the elastic and viscous behavior of bitumen. It's able to perform tests on different temperatures and frequencies.

Throughout torque, the DSR subjects a binder sample to shear loading. The load is applied sinusoidally. It's possible to calculate the strain and stress by means of eq. 44 and eq. 45 respectively.

The binder sample is positioned between a superior and an inferior plate (fig. 6 b). The superior plate rotates while the inferior plate remains still.

$$\tau = \frac{2 \cdot T}{\pi \cdot R^3} \tag{44}$$

$$\gamma = \frac{\varphi \cdot R}{h} \tag{45}$$

Where, T is torque, R the plate radious, φ the rotation angle and h the distance between the superior and inferior plate.

For the purpose of this work, an 8 mm diameter plate was used and a separation of 2 mm between the plates in all cases.
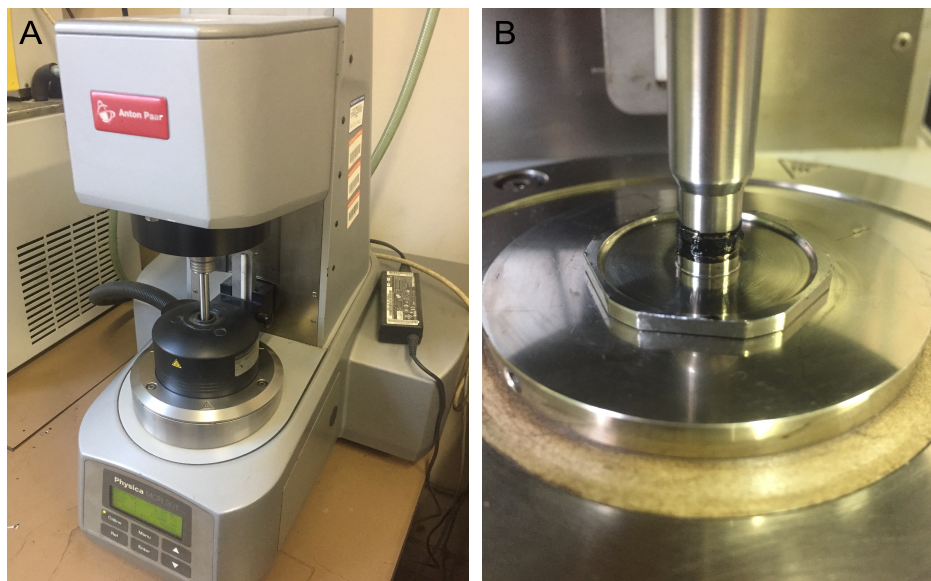
Fig. 6. A) Rheometer; B) Superior and inferior plate

2.2 Materials

In this work, four different binders were studied: Feyzin, Mantova, PG − 64 - 22 and PG − 76 − 16 in their original state. The last two were also studied in their PAV state.

A SARA analysis was performed in all binders. This test provides information regarding the percentage of saturates, aromatics, resins and asphaltenes present in the binders.
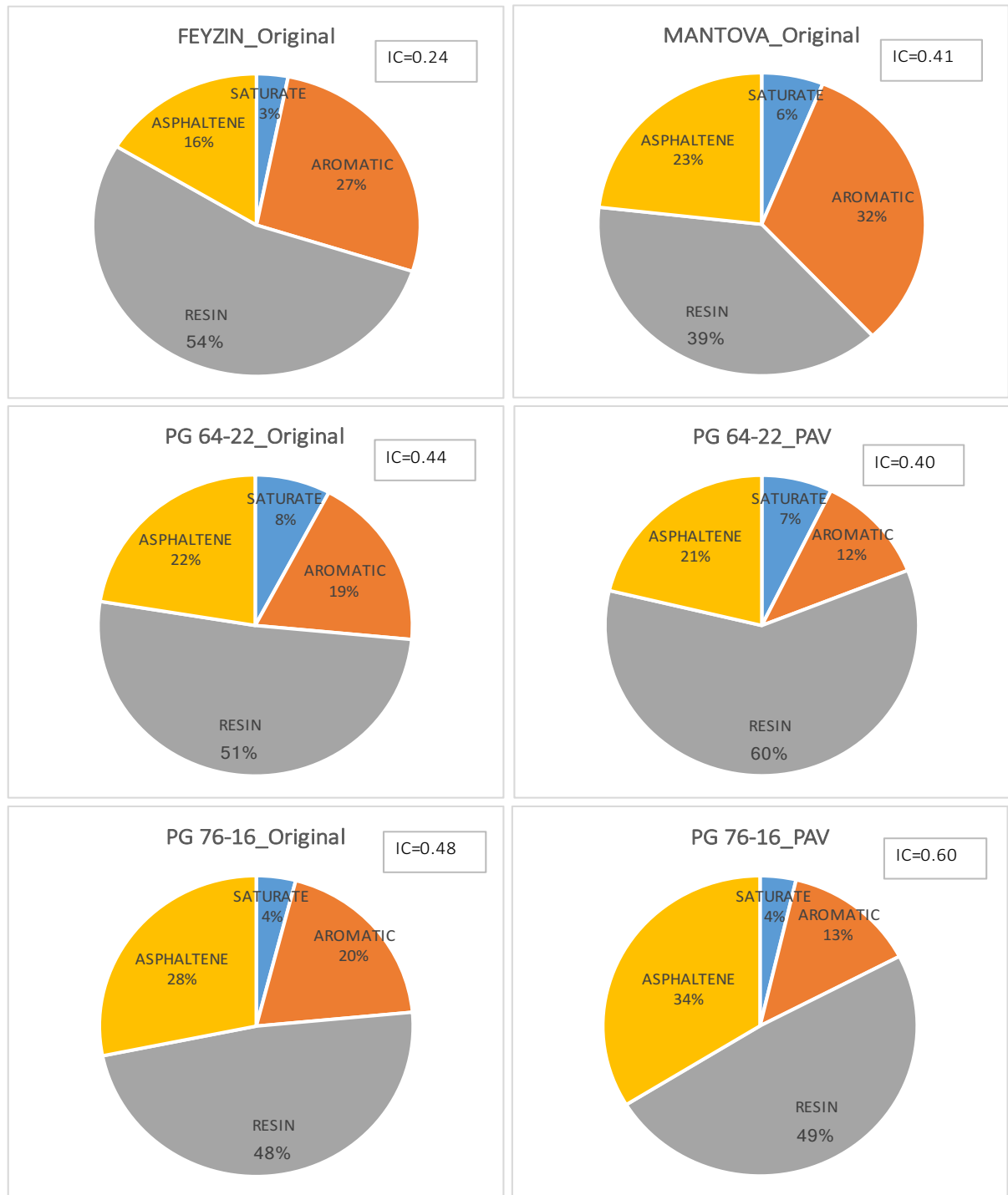
Fig. 7. SARA analysis

In fig. 7, $I_C = (aromatics + resisns)/(asphaltenes + saturates)$ is the index of colloidal stability.

A high I_C indicates that that the binder is a GEL system. This means that there are not enough resins to maintain asphaltenes highly dispersed in the oily phase. Therefore, GEL systems have a Newtonian behavior.

On the other hand, a low I_C indicates that the binder is a SOL system. In this case resins aren't effective on the peptization of asphaltenes. Consequently, SOL systems don't have a Newtonian behavior. In our case, only Feyzin is a SOL system.

2.3 Testing protocol

The first step of all tests is the dumping of bitumen into the container presented in fig 8.
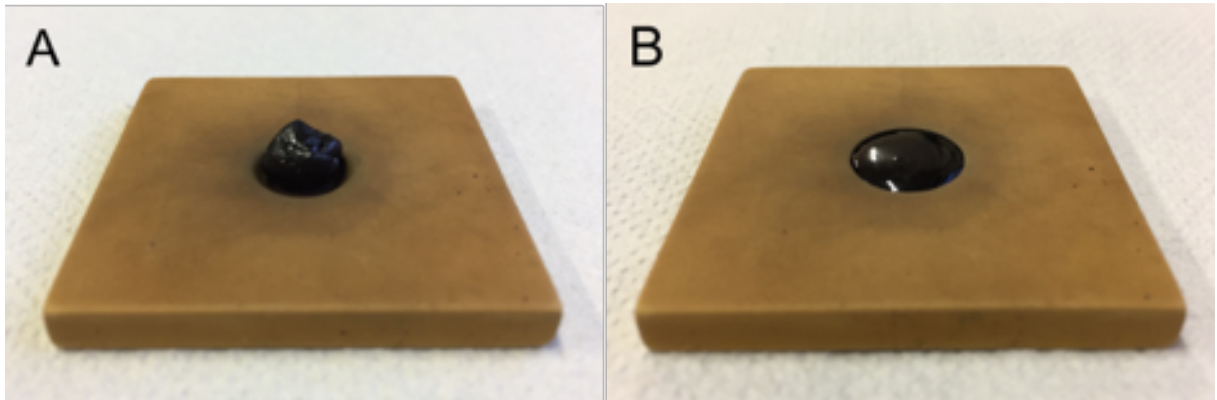
Fig. 8. A) bitumen dumped in the container. B) bitumen in the container after it has been in the oven

Afterwards the loaded container is introduced into an oven were it remains at 150°C for 10 minutes. Then, the sample is taken out of the oven and left at room temperature (approximately 21°C) for 5 minutes. After this, it's put into a freezer at -6°C for 3 minutes. Once the sample is positioned on the inferior plate, the upper plate goes to the trimming position where the distance between both plates is 2,1 mm (fig. 9).
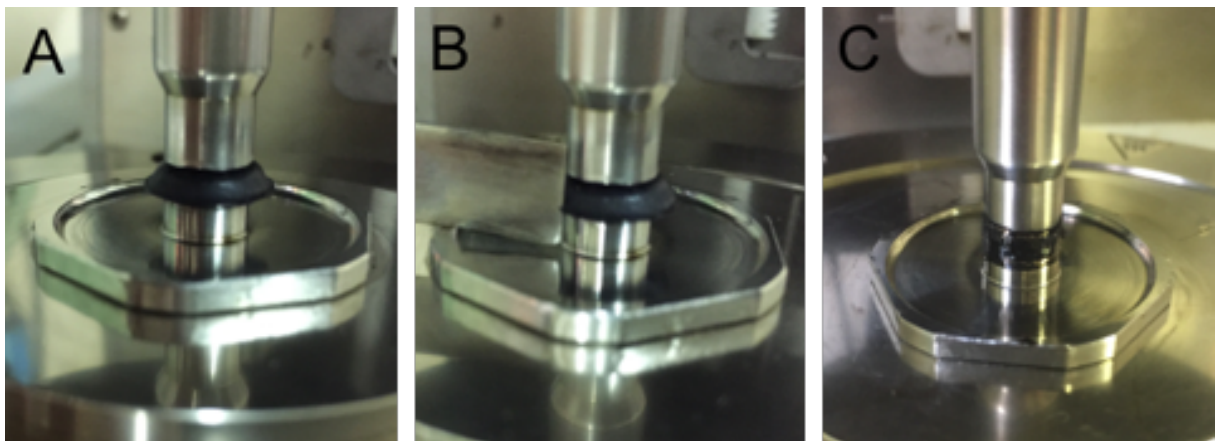
Fig. 9. A) Sample before trimming. B) Sample being trimmed. C) Sample after trimming

The sample is then trimmed by means of a scraper (fig. 10). During this phase, the plates are at 45°C.

Fig. 10. Scrapers

After the trimming is finished, the plate goes to the test position where the distance between both plates is 2,0 mm. Then, the sample cover of the rheometer goes down in order to maintain a constant temperature during the tests (fig. 11). Afterwards, the test begins.
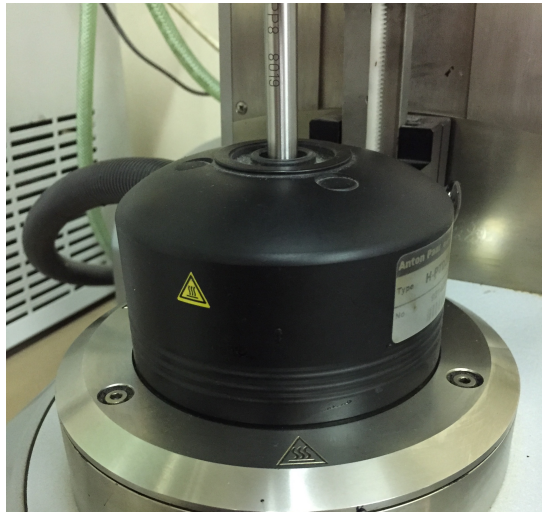
Fig. 11. Sample cover

In all cases, the sample undergoes a conditioning process of 35 minutes at the beginning of the test.

2.4 Amplitude sweep test

Bitumen behaves like a linear viscoelastic material only within a certain strain range. This range varies according to temperature and loading frequency.
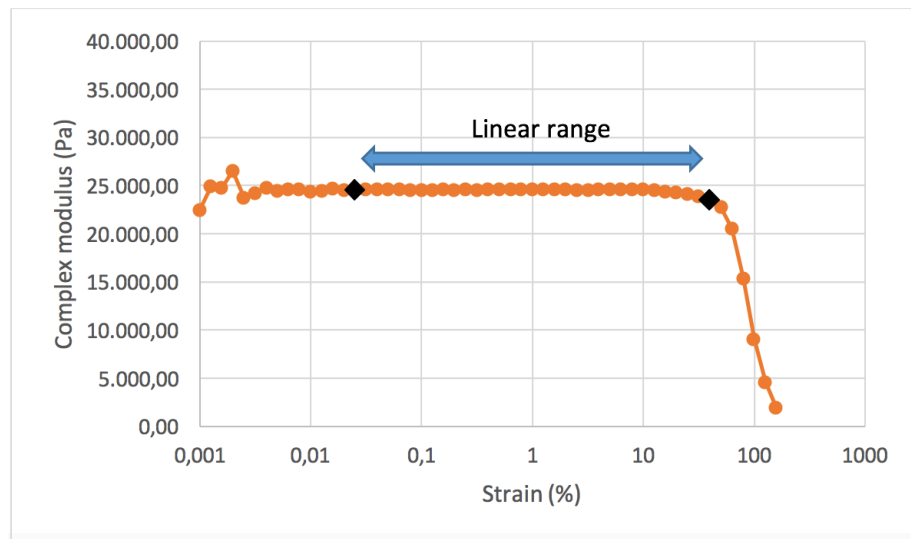
Fig. 12. Amplitude sweep test

Fig. 12 shows the results from an amplitude sweep test. We can see a reduction of the complex modulus outside the linear range as the strain increases. The upper limit of the linear range is determined when a reduction of 5% of the modulus is reached. On the other hand, the inferior limit is placed where the modulus stabilizes at constant value, after the initial variability that can be seen when the strain is small.

The amplitude sweep test is performed at different temperatures and loading frequencies for the purpose of describing how the limits of the range vary depending on the reduced frequency (fig. 13).
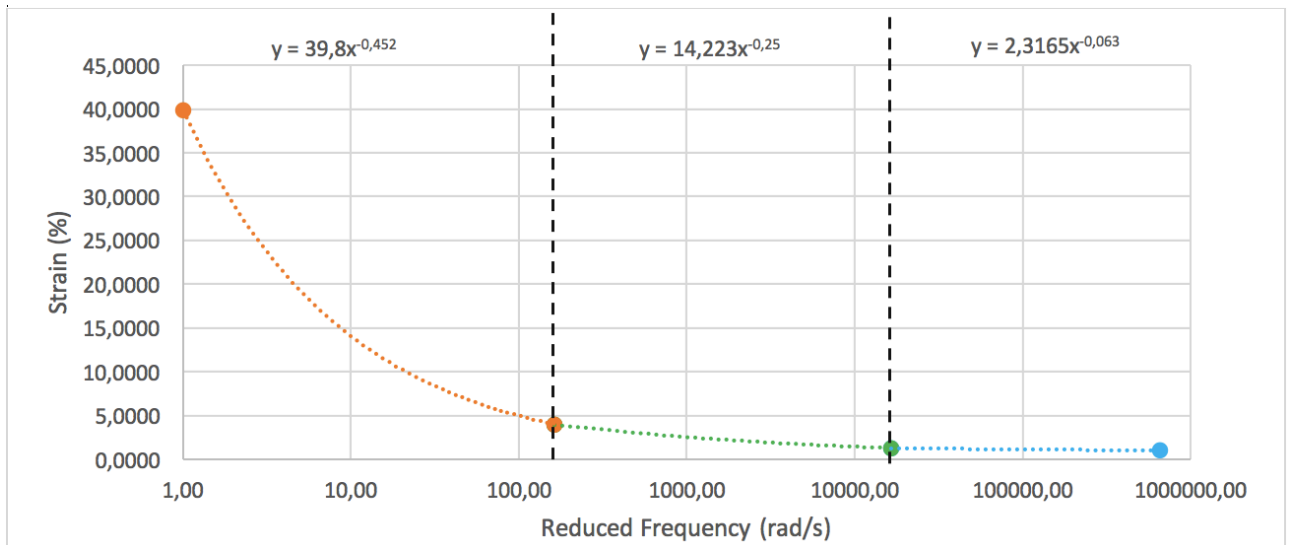
Fig. 13. Example of the upper limit of the linear range

2.5 Frequency sweep test

This test provides the necessary information for the construction of the master curves (fig. 14).
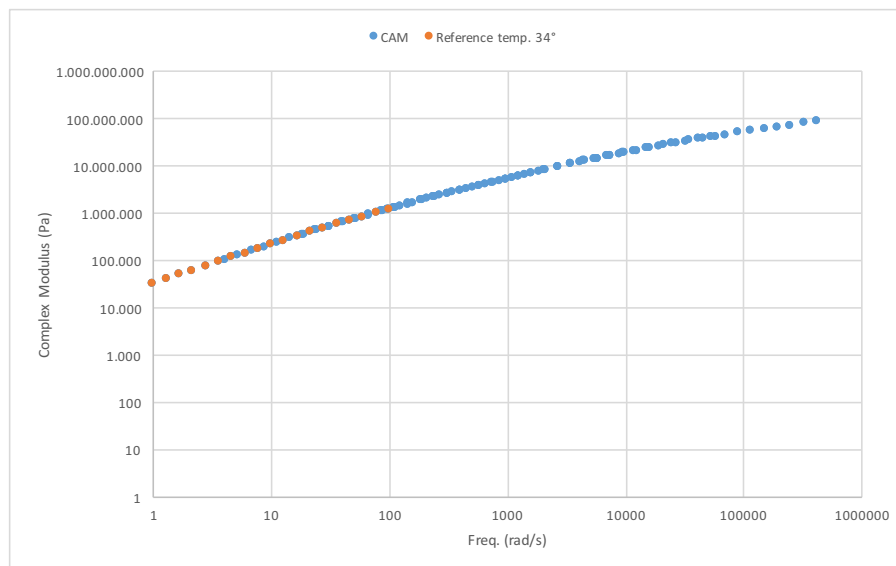
Fig. 14. Master curve

The frequency sweep test (FST) is performed in steps. On each step the frequency varies while the temperature remains constant. An example of the raw data obtained from this test can be seen on the fig. 15.
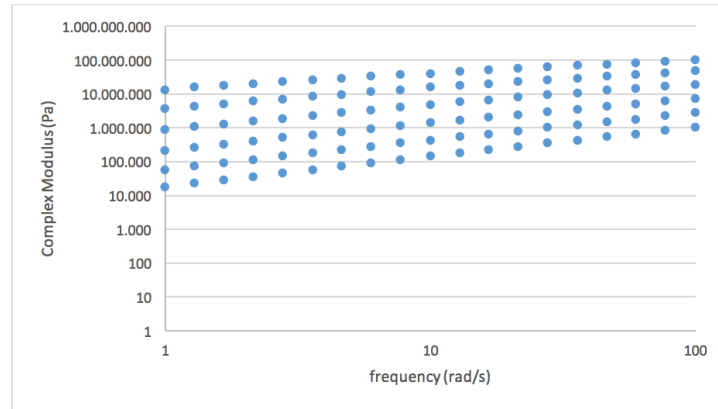
Fig. 15. Raw data FST

By means of the shift factors and the CAM model the curves on fig. 15 can be horizontally moved in order to obtain the master curve (fig. 1, section 1.1.4).

The FST is performed entirely within the linear range of the material.

2.6 Multiple strain sweep

Outside the linear range, a reduction of the complex modulus can be observed as the strain applied to the material is increased. This reduction is due to nonlinear behaviour and damage. In order to distinguish damage from nonlinearity Underwood (Underwood & Kim, 2014) proposes a method that consists in a series of loading groups with an increasing stress – strain level. Each group has three equal loading blocks (fig. 16).
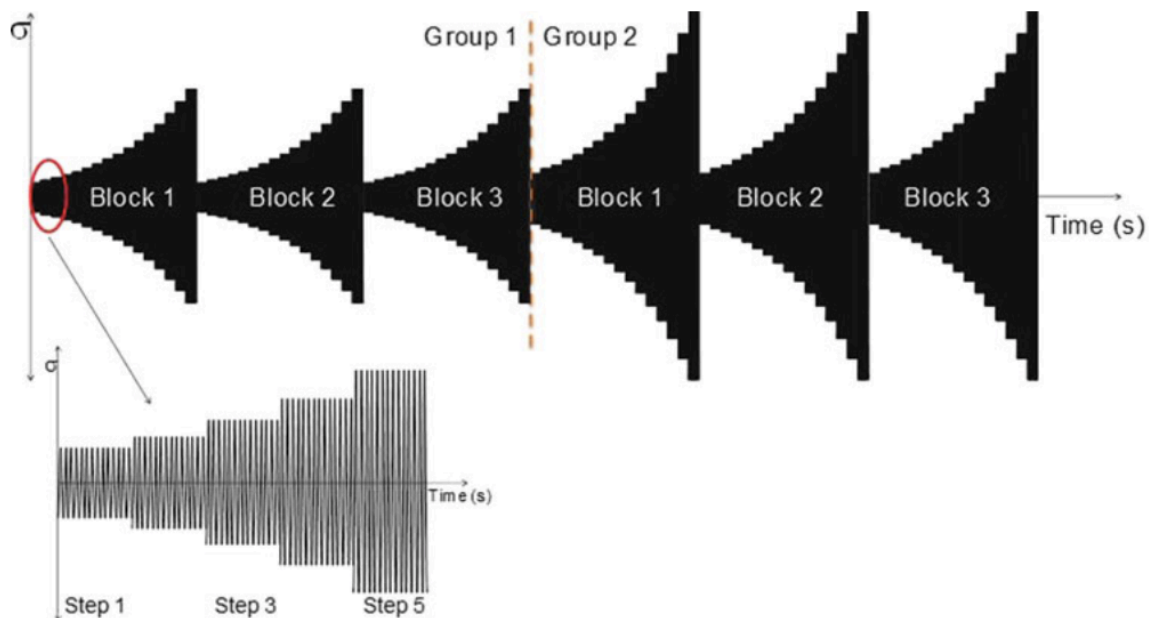
Fig. 16. (Underwood & Kime, 2014)

The first group is within the linear range. From the second group damage and nonlinearity can be observed.

One of the most important hypothesis of the method consist in considering that, when there's damage, it's only generated on the first block of each group (G2B1 on fig. 17), in other words, there is damage only when a certain level of strain is reached for the first time.

The previous hypothesis is the key for distinguishing damage from nonlinearity.
In fact, what was done, is a vertical shift of the curve of the second block of the second group (G2B2 on fig. 17) to the value of the linear modulus (G1B1 on fig. 17).
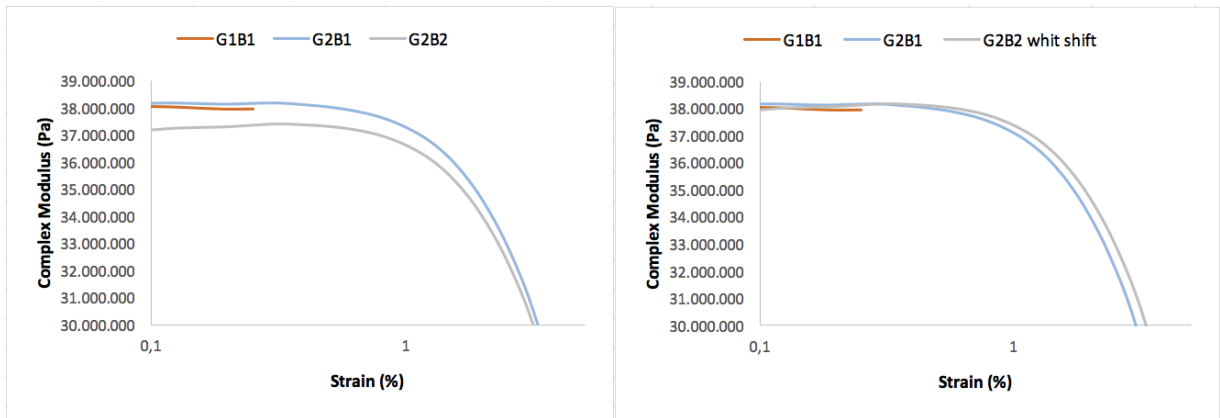
Fig. 17. Isolation of damage from nonlinearities

This is how the non-linear viscoelastic curve is obtained (G2B2 with shift, on fig. 17). This curve is free of damage.
This test was performed at different temperatures: 34, 28, 22, 16 and 10 °C; with a loading frequency of 10 Hz.
At each strain level, it's possible to approximate a strain dependent master curve thanks to the 5 points obtained from the multiple strain tests performed at 5 different temperatures (fig. 18). It's important to point out that the temperature shift factors $a(T)$ are also valid in the non linear range (section 1.3.3).
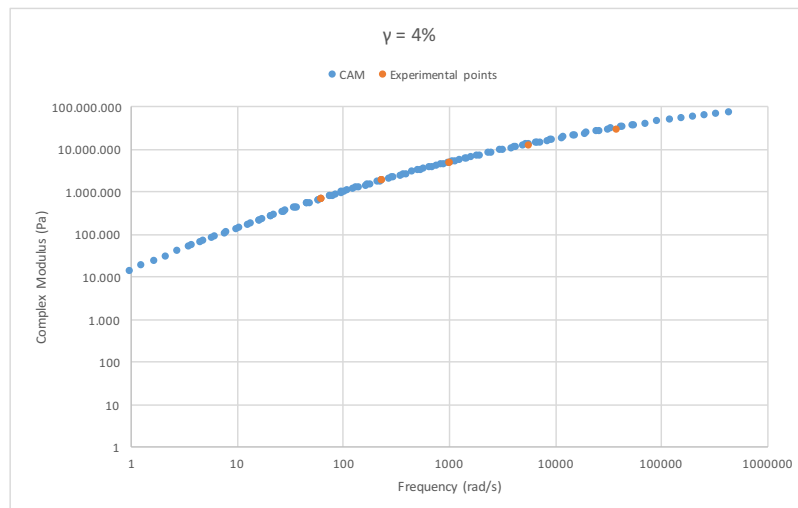
Fig. 18. Master curve obtained for a 4% strain

Once we have the strain dependent master curves, it's possible to obtain the a_γ and h_1 shift factors (section 1.2.6) at each strain level. Afterwards, by means of a regression model, a model for both shift factors is obtained (fig. 19). This model describes how the shift factors vary as a function of strain.
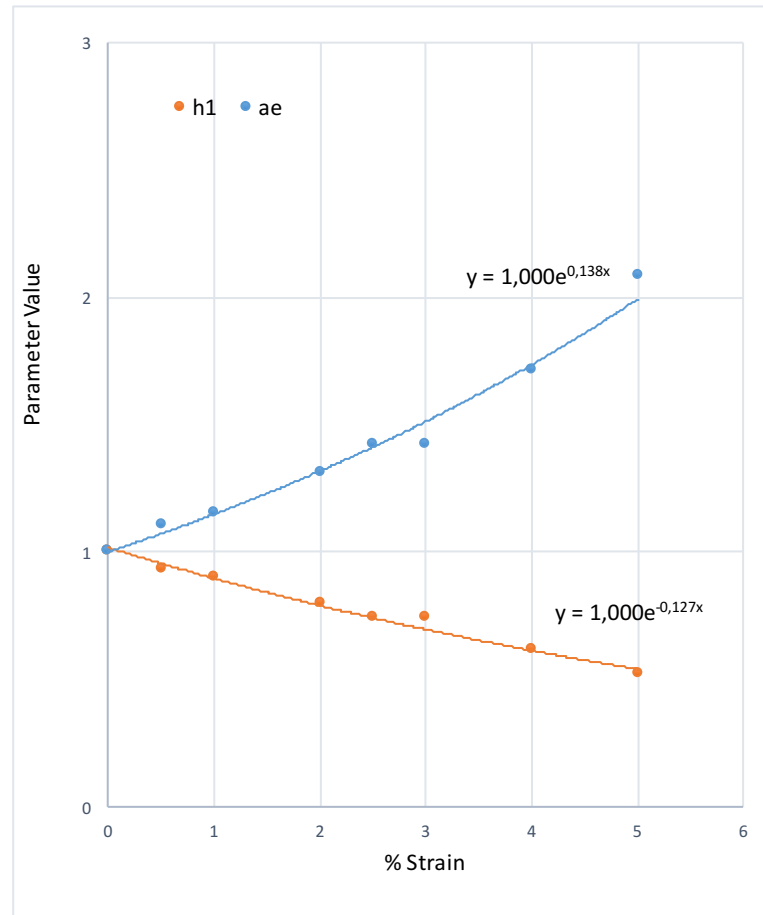
Fig. 19. a_γ and h_1 models for the Feyzin binder

2.7 Time sweep test

This test submits a binder sample to a sinusoidal load maintaining a constant strain amplitude. On each material, it was performed at three different strain levels. After a certain number of loading cycles, the complex modulus decreases due to fatigue (fig. 20). The test finishes when the complex modulus reaches a 10% of its original value.
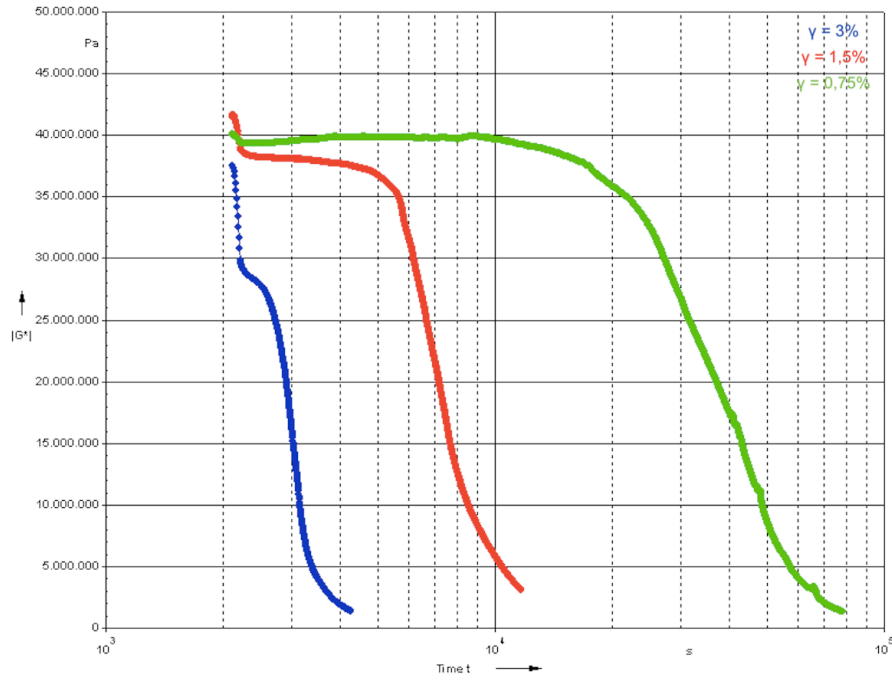
Fig. 20. Complex modulus vs. time

Due to the fact that this is a strain controlled test, a reduction of the loading stress can be observed as the test evolves (fig. 21).
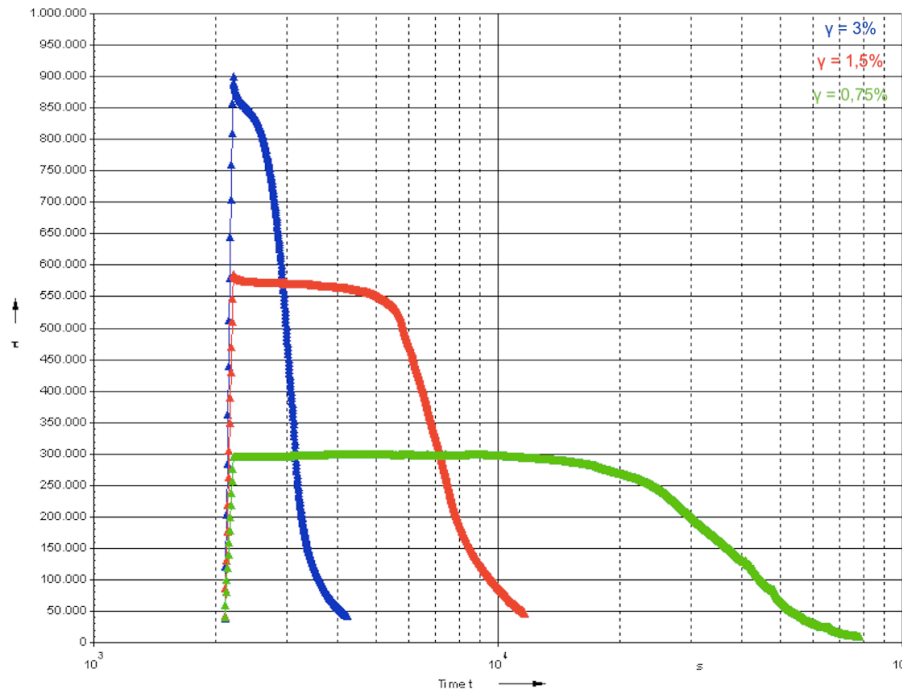
Fig. 21. Stress vs. time

The reduction in the stress allows the calculation of the pseudo stiffness and damage (section 1.3). Afterwards, the C vs S curve is obtained (fig. 22). As explained in the previous chapter, this curve is independent of the stain amplitude.
This curves are approximated with a regression model (eq. 43), (fig. 22).
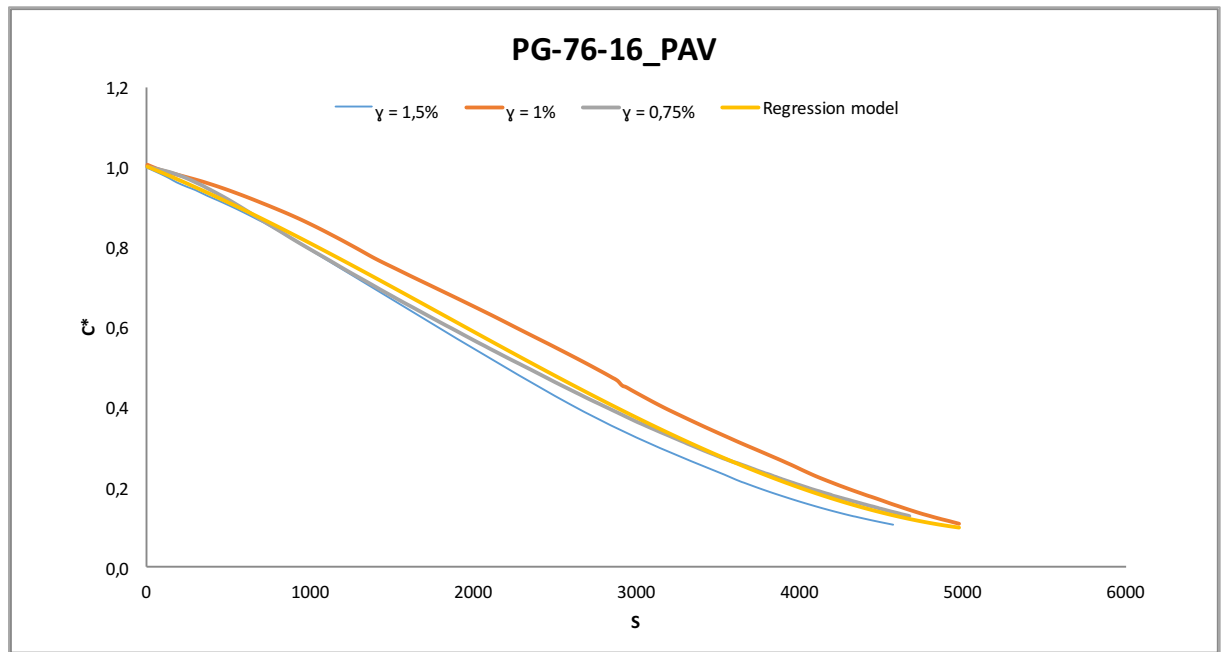
Fig. 22. PG-76-16_PAV damage characteristic curve

Chapter 3: Results

3.1 Linear viscoelastic range limits

3.1.1 Upper linear viscoelastic limit

As explained in section 2.4, the limits of the linear range variate as a function of the reduced frequency (fig. 13). This variation was modeled with an exponential function (eq. 46).

$$\gamma(\%) = a \cdot e^{b} \tag{46}$$

The parameter values are presented in table 1. These parameters are valid only within a certain reduced frequency range, as specified in the table.

Reduced freq. range [rad/s]	Function parameters (eq. 46)	FEYZIN	MANTOVA	PG-64-22 Original	PG-64-22 PAV	PG-76-16 Original	PG-76-16 PAV
1,0 – 163,9	a	39,800	1,260	31,600	6,310	10,000	2,510
	b	-0,452	0,135	-0,361	-0,226	-0,226	-0,091
163,9 – 16390,7	a	14,223	6,954	29,838	4,264	11,298	2,622
	b	-0,250	-0,200	-0,350	-0,149	-0,250	-0,099
16390,7 - 651899,6	a	2,316	1,000	1,830	1,830	1,830	3,350
	b	-0,063	0,000	-0,062	-0,062	-0,062	-0,125

Table 1

3.1.2 Inferior linear viscoelastic limit

The inferior linear viscoelastic limit was also modeled with an exponential function (eq. 46). The parameters values are presented in table 2.

Reduced freq. range [rad/s]	Function parameters (eq. 46)	FEYZIN	MANTOVA	PG-64-22 Original	PG-64-22 PAV	PG-76-16 Original	PG-76-16 PAV
1,0 – 163,9	a	0,040	0,005	0,020	0,025	0,025	0,013
	b	-0,136	0,045	-0,090	-0,226	-0,226	-0,091
163,9 – 16390,7	a	0,0257	0,014	0,035	0,017	0,022	0,017
	b	-0,050	-0,150	-0,200	-0,150	-0,200	-0,150
16390,7 - 651899,6	a	3,711	0,006	0,105	0,276	0,120	0,024
	b	-0,563	-0,063	-0,313	-0,437	-0,375	-0,187

Table 2

3.2 Viscoelastic models

3.2.1 CAM model

By means of the frequency sweep test (section 2.5) and the formulae presented in section 1.2.5 a CAM model was obtained for each binder. The parameters of the models are presented in table 3.

CAM parameters (eq. 46)	FEYZIN	MANTOVA	PG-64-22 Original	PG-64-22 PAV	PG-76-16 Original	PG-76-16 PAV
C1	11,201	16,281	15,142	30,777	17,134	26,690
C2	122,216	164,363	155,440	271,239	167,173	233,032
log(Gg) [Pa]	8,703	8,809	8,861	9,157	8,990	9,254
log(wc) [rad/s]	3,972	3,390	3,675	0,000	3,643	1,724
R	1,320	2,022	1,661	2,791	1,778	2,809
m	1,073	1,067	1,052	1,314	0,958	0,827

Table 3

3.2.2 Prony series

By means of collocation the modules of the Maxwell elements (G_m) were obtained (section 1.2.4). The results are presented in table 4.

ρ_m	ω	G_m [Pa]					
[s]	[rad/s]	FEYZIN	MANTOVA	PG-64-22 Original	PG-64-22 PAV	PG-76-16 Original	PG-76-16 PAV
0,00000002	0,00000002	5,10E+07	4,99E+07	6,48E+07	6,58E+07	8,14E+07	8,14E+07
0,00000006	0,00000006	4,91E+07	3,47E+07	5,30E+07	4,84E+07	6,13E+07	6,13E+07
0,0000002	0,0000002	4,30E+07	2,71E+07	4,39E+07	3,88E+07	4,94E+07	4,94E+07
0,0000006	0,0000006	4,68E+07	2,40E+07	4,32E+07	3,80E+07	5,00E+07	5,00E+07
0,000002	0,000002	3,52E+07	1,61E+07	3,08E+07	2,73E+07	3,64E+07	3,64E+07
0,000006	0,000006	3,03E+07	1,25E+07	2,55E+07	2,47E+07	3,45E+07	3,45E+07
0,00002	0,00002	1,90E+07	7,51E+06	1,60E+07	1,67E+07	2,41E+07	2,41E+07
0,00006	0,00006	1,22E+07	4,99E+06	1,08E+07	1,37E+07	2,11E+07	2,11E+07
0,0002	0,0002	6,07E+06	2,67E+06	5,74E+06	8,66E+06	1,40E+07	1,40E+07
0,0006	0,0006	2,86E+06	1,51E+06	3,12E+06	6,33E+06	1,13E+07	1,13E+07
0,002	0,002	1,11E+06	7,15E+05	1,40E+06	3,68E+06	7,08E+06	7,08E+06
0,006	0,006	3,88E+05	3,45E+05	6,14E+05	2,37E+06	5,23E+06	5,23E+06
0,02	0,02	1,21E+05	1,45E+05	2,35E+05	1,25E+06	3,09E+06	3,09E+06
0,06	0,06	3,21E+04	6,04E+04	8,46E+04	7,04E+05	2,09E+06	2,09E+06
0,2	0,2	8,26E+03	2,28E+04	2,81E+04	3,34E+05	1,16E+06	1,16E+06
0,6	0,6	1,56E+03	8,32E+03	8,54E+03	1,62E+05	7,25E+05	7,25E+05

ρ_m	ω	G_m					
		[Pa]					
[s]	[rad/s]	FEYZIN	MANTOVA	PG-64-22 Original	PG-64-22 PAV	PG-76-16 Original	PG-76-16 PAV
2	2	3,22E+02	2,87E+03	2,53E+03	6,83E+04	3,80E+05	3,80E+05
6	6	-2,11E+01	9,34E+02	6,52E+02	2,83E+04	2,18E+05	2,18E+05
20	20	-1,38E+01	2,98E+02	1,73E+02	1,05E+04	1,08E+05	1,08E+05
60	60	2,61E+00	8,80E+01	3,66E+01	3,67E+03	5,79E+04	5,79E+04
200	200	-3,50E-01	2,64E+01	7,97E+00	1,19E+03	2,72E+04	2,72E+04
600	600	5,53E-02	7,10E+00	1,27E+00	3,34E+02	1,37E+04	1,37E+04
2000	2000	-7,26E-03	2,01E+00	-2,55E-01	8,98E+01	6,16E+03	6,16E+03
6000	6000	1,15E-03	4,89E-01	-1,33E-02	1,66E+01	2,94E+03	2,94E+03
20000	20000	-1,51E-04	1,29E-01	3,26E-03	3,62E+00	1,27E+03	1,27E+03
60000	60000	2,38E-05	2,73E-02	-5,38E-04	-2,03E+00	5,81E+02	5,81E+02
200000	200000	-3,12E-06	6,26E-03	7,10E-05	3,05E-01	2,43E+02	2,43E+02
600000	600000	4,93E-07	9,76E-04	-1,12E-05	-4,88E-02	1,09E+02	1,09E+02
2000000	2000000	-6,47E-08	9,41E-06	1,47E-06	6,41E-03	4,24E+01	4,24E+01
6000000	6000000	1,02E-08	-6,95E-05	-2,32E-07	-1,01E-03	2,14E+01	2,14E+01
20000000	20000000	-1,31E-09	1,07E-05	2,97E-08	1,29E-04	4,09E+00	4,09E+00
60000000	60000000	1,66E-10	-1,38E-06	-3,78E-09	-1,65E-05	7,43E+00	7,43E+00

Table 4

3.2.3 Non-linear viscoelastic shift factors

By means of the multiple strain sweep tests (MSS), the distinction of the non-linear behavior from damage was achieved (section 2.6). The first step of this process was the procurement of the mastercurves associated to different strain levels. These were obtained by approximating CAM models to the experimental points obtained in the MSS tests (Appendix), as seen in figure 23.
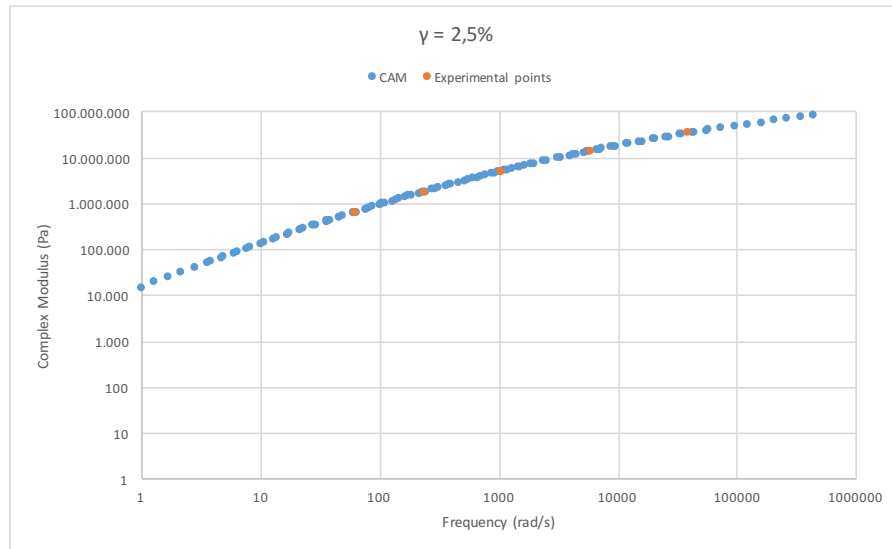The CAM model parameters are presented in table 6.

Fig. 23. Feyzin matercurve obtained for a 2,5% strain

Binder	CAM parameters	γ = 0,5 %	γ = 1 %	γ = 2 %	γ = 2,5 %	γ = 3 %	γ = 4 %	γ = 5 %
FEYZIN	log(Gg) [Pa]	8,70	8,70	8,70	8,70	8,70	8,70	8,70
	log(wc) [rad/s]	3,98	3,89	3,43	3,01	2,93	1,93	1,19
	R	1,33	1,36	1,48	1,58	1,60	1,79	1,93
	m	1,07	1,09	1,18	1,28	1,30	1,57	1,78
MANTOVA	log(Gg) [Pa]	8,81	8,81	8,81	8,81	8,81	8,81	8,81
	log(wc) [rad/s]	3,42	3,28	2,96	2,67	2,50	2,02	0,98
	R	2,02	2,06	2,18	2,26	2,30	2,49	2,72
	m	1,06	1,08	1,12	1,15	1,18	1,22	1,37
PG - 64 - 22 Original	log(Gg) [Pa]	8,86	8,86	8,86	8,86	8,86	8,86	8,86
	log(wc) [rad/s]	3,67	3,54	2,95	2,43	1,78	0,01	0,00
	R	1,66	1,70	1,84	1,95	2,07	2,35	2,47
	m	1,05	1,08	1,18	1,28	1,42	1,86	1,74
PG - 64 - 22 PAV	log(Gg) [Pa]	9,16	9,16	9,16	9,16	9,16	9,16	9,16
	log(wc) [rad/s]	0,00	0,00	0,00	0,00	0,00	0,00	0,00
	R	3,01	3,04	3,15	3,22	3,22	3,39	3,61
	m	1,19	1,17	1,13	1,10	1,10	1,04	0,97
PG - 76 - 16 Original	log(Gg) [Pa]	8,99	8,99	8,99	8,99	8,99	8,99	8,99
	log(wc) [rad/s]	3,53	3,32	2,69	2,03	1,97	0,68	0,00
	R	1,80	1,85	2,01	2,14	2,21	2,45	2,66
	m	0,98	1,01	1,11	1,22	1,21	1,44	1,50
PG - 76 - 16 PAV	log(Gg) [Pa]	9,25	9,25	9,25	9,25	9,25	9,25	9,25
	log(wc) [rad/s]	1,59	1,03	1,25	0,52	0,28	0,00	0,00
	R	2,84	2,96	3,02	3,20	3,35	3,50	3,71
	m	0,84	0,89	0,84	0,90	0,89	0,90	0,85

Table 5

From the mastercurves obtained for the different strain levels, the non-linear shift factors a_γ and h_1 were obtained (section 1.2.6). Data presented in table 6.

Binder	Shift factor	γ = 0,5 %	γ = 1 %	γ = 2 %	γ = 2,5 %	γ = 3 %	γ = 4 %	γ = 5 %
FEYZIN	a_γ	1,107	1,150	1,308	1,419	1,420	1,710	2,085
	h_1	0,934	0,903	0,800	0,739	0,739	0,615	0,518
MANTOVA	a_γ	1,064	1,143	1,552	1,860	1,978	3,246	4,715
	h_1	0,992	0,938	0,746	0,650	0,621	0,423	0,321
PG - 64 - 22 Original	a_γ	1,019	1,064	1,276	1,452	1,659	2,420	4,150
	h_1	0,991	0,957	0,827	0,747	0,672	0,511	0,358
PG - 64 - 22 PAV	a_γ	1,015	1,130	1,592	1,996	2,388	3,769	7,087
	h_1	0,993	0,935	0,763	0,667	0,595	0,453	0,320
PG - 76 - 16 Original	a_γ	1,013	1,070	1,368	1,598	2,019	2,850	4,975
	h_1	0,993	0,952	0,795	0,707	0,604	0,475	0,334
PG - 76 - 16 PAV	a_γ	1,096	1,303	1,664	2,234	3,348	4,316	7,671
	h_1	0,966	0,889	0,755	0,647	0,532	0,442	0,326

Table 6

From the data presented in table 6, regression models were created in order to predict the shift factors value as a function of the strain, as shown in fig. 24.
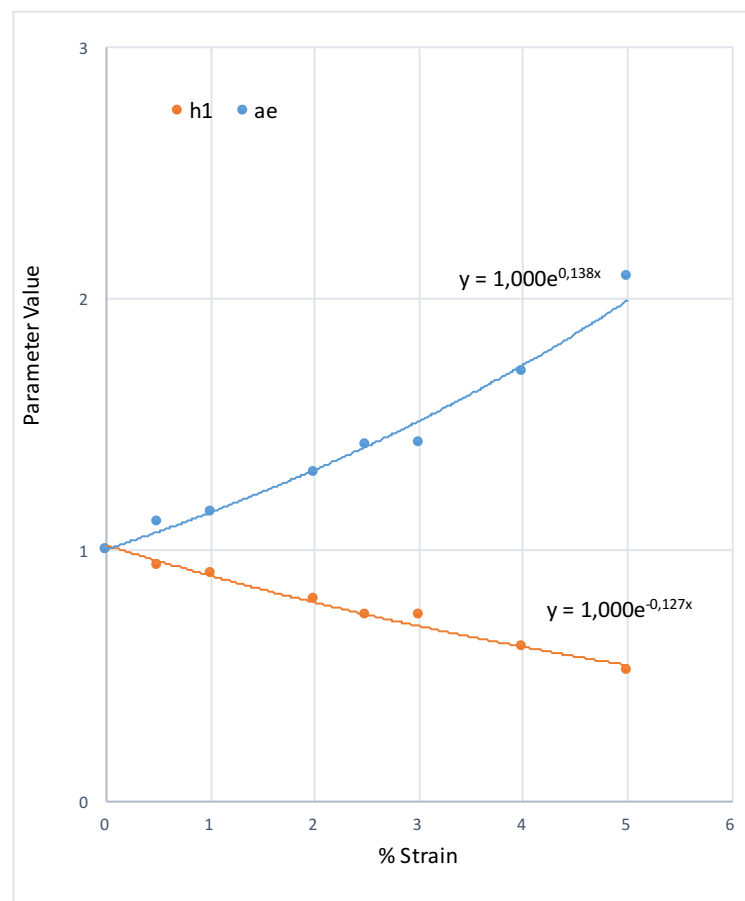

Fig. 24. FEYZIN Shift factors regression model

In some cases, the best approaching function was an exponential function (eq. 47), in some others, a second degree polynomial or a third degree polynomial (eq. 48). The Regression parameters are presented in table 7.

$$y = a \cdot e^{b \cdot \gamma (\%)} \tag{47}$$

$$y = c \cdot \gamma(\%)^3 + d \cdot \gamma(\%)^2 + e \cdot \gamma(\%) + f \tag{48}$$

Binder	Shift factor	Regression model parameters					
		a	b	c	d	e	f
FEYZIN	a_γ	1,000	0,138				
	h_1	1,000	-0,127				
MANTOVA	a_γ			0,020	0,025	0,128	1,000
	h_1			0,007	-0,054	-0,042	1,000
PG - 64 - 22 Original	a_γ			0,017	0,008	0,052	1,000
	h_1			0,007	-0,062	0,009	1,000
PG - 64 - 22 PAV	a_γ			-0,012	0,219	-0,085	1,000
	h_1			0,021	-0,119	0,035	1,000
PG - 76 - 16 Original	a_γ			0,003	0,122	-0,067	1,000
	h_1			0,008	-0,064	-0,004	1,000
PG - 76 - 16 PAV	a_γ				0,207	0,029	1,000
	h_1			0,012	-0,078	-0,025	1,000

Table 7

In fig. 25, a representation of the non-linear shift factors models of the studied binders in their original state is presented.
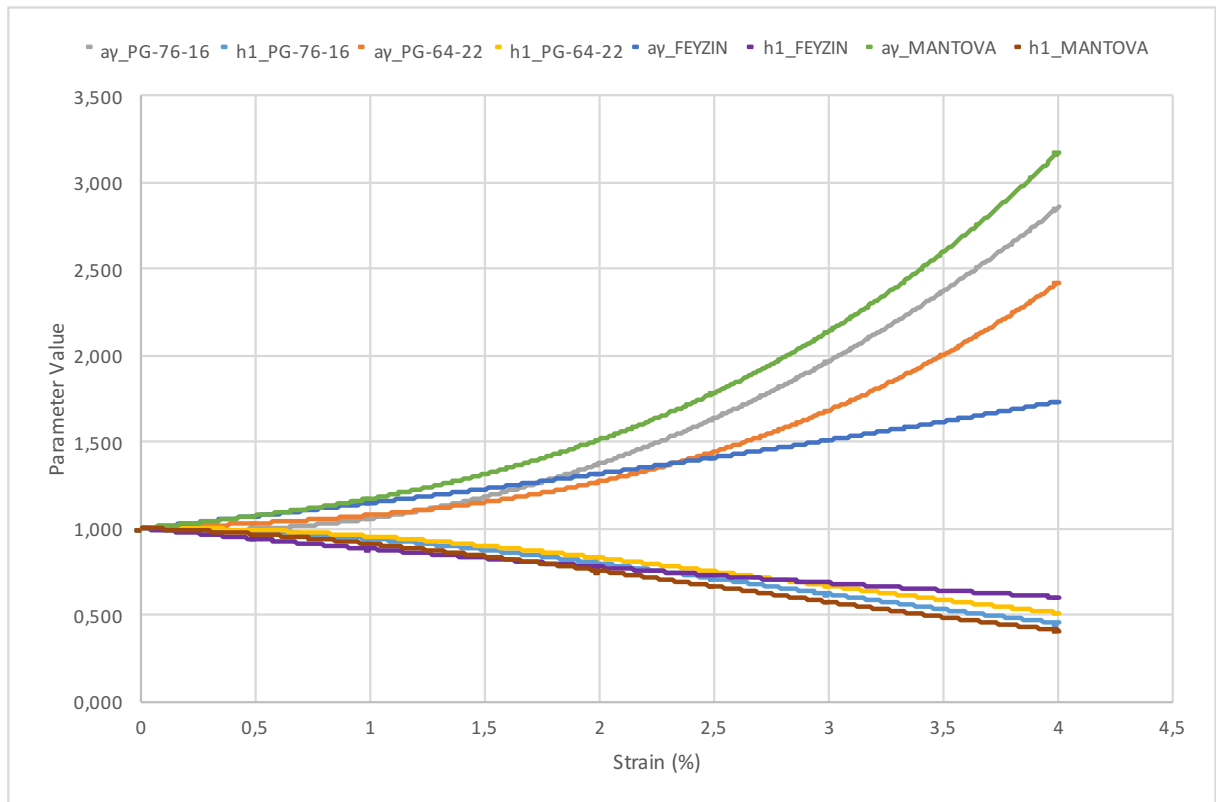
Fig. 25. Non-linear shift factors of binders in their original state

Mantova is the binder with the strongest non-linear behavior due to the fact that for a certain strain level it has the highest a_γ and the lowest h_1. On the other hand, the binder with the

weakest non-linear behavior is the PG-64-22 for strains under approximately 2,5% and FEYZIN for strains over 2,5%.

It's important to point out that there are small differences between the models of the different binders that approximate the h_1 shift factor.

3.2.4 Effect of aging on the non-linear behavior

Fig. 26. Effect of aging on the non-linear shift factors, PG-64-22

Fig. 27. Effect of aging on the non-linear shift factors, PG-76-16

As seen in fig. 26 and 27, the aging process modify the bitumen non-linear shift factors. This effect is more considerable in the a_γ shift factor than in the h_1 shift factor.
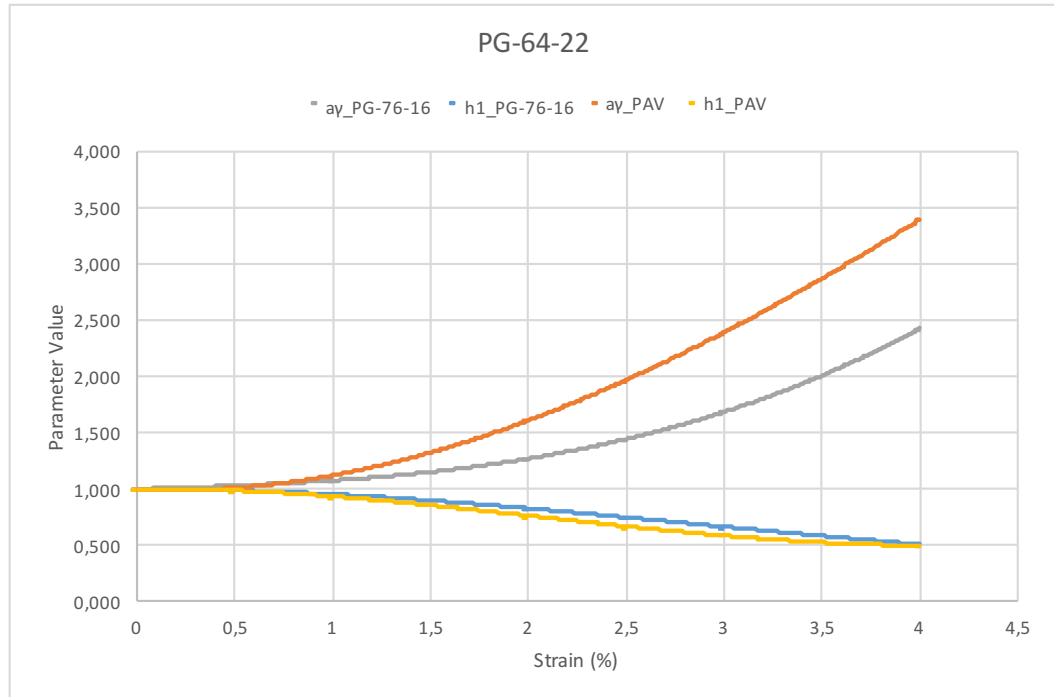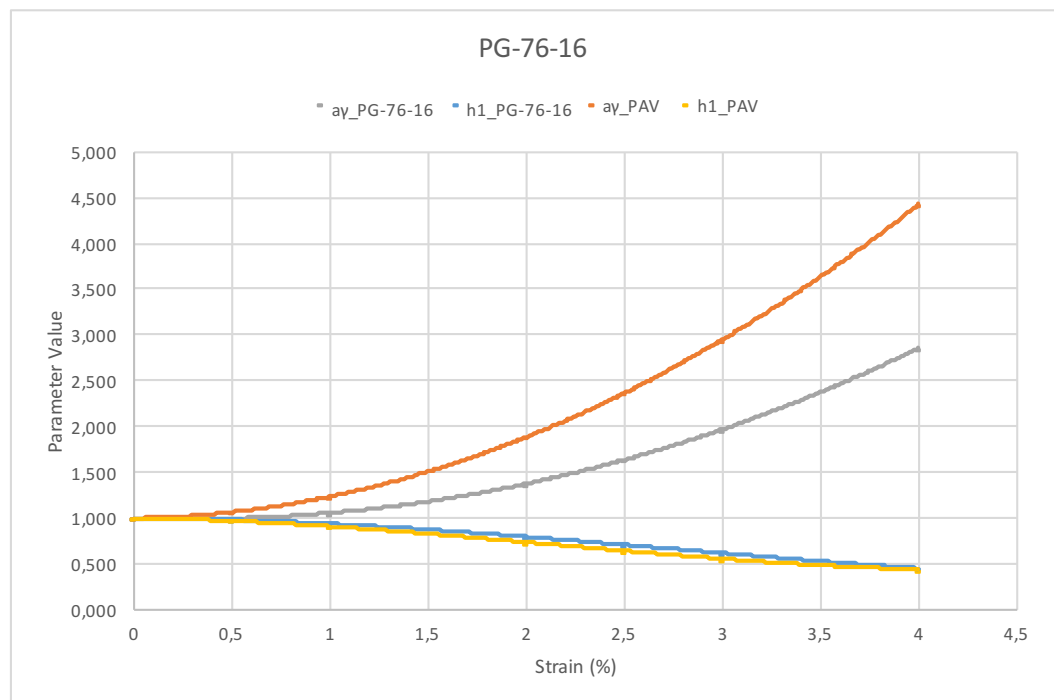
For the same strain level, a_γ is higher and h_1 lower in the aged bitumen in comparison to the same bitumen in its original state. This indicates that the non-linear behavior appears at lower strains in the aged bitumen and that explains why its linear range is smaller, in other words, the nonlinear behavior is evident at lower levels of strains in comparison to the original binders.

3.2 Damage characteristic curves

The damage characteristic curve was obtained for three different strain levels (fig. 28-33). Afterwards, the experimental curves were approximated with a regression model. The function used for the approximation is a third degree polynomial (eq. 49). The parameter values are shown in table 8.

$$C^* = a \cdot S^3 + b \cdot S^2 + c \cdot S + d \tag{49}$$

Binder	Damage characteristic curves, regression parameters			
	a	b	c	d
FEYZIN	1,95E-11	-7,23E-08	-2,65E-04	1,00E+00
MANTOVA*	-4,79E-11	7,46E-08	-3,93E-04	9,32E-01
PG - 64 - 22 Original	1,46E-11	-7,71E-08	-1,66E-04	1,00E+00
PG - 64 - 22 PAV	3,75E-11	-1,47E-07	-1,92E-04	1,00E+00
PG - 76 - 16 Original	2,08E-11	-1,12E-07	-9,90E-05	1,00E+00
PG - 76 - 16 PAV	2,08E-11	-1,12E-07	-9,90E-05	1,00E+00

*Table 8. *The Mantova polynomial is only valid for S > 250.*

For the purpose of a better approximation, the Mantova regression model was divided into two parts. The polynomial presented in table 8 is only valid for S > 250. For S < 250, eq. 50 is used.

$$C^* = 1,0000 - 0,0115 \cdot S^{0,4795} \tag{50}$$
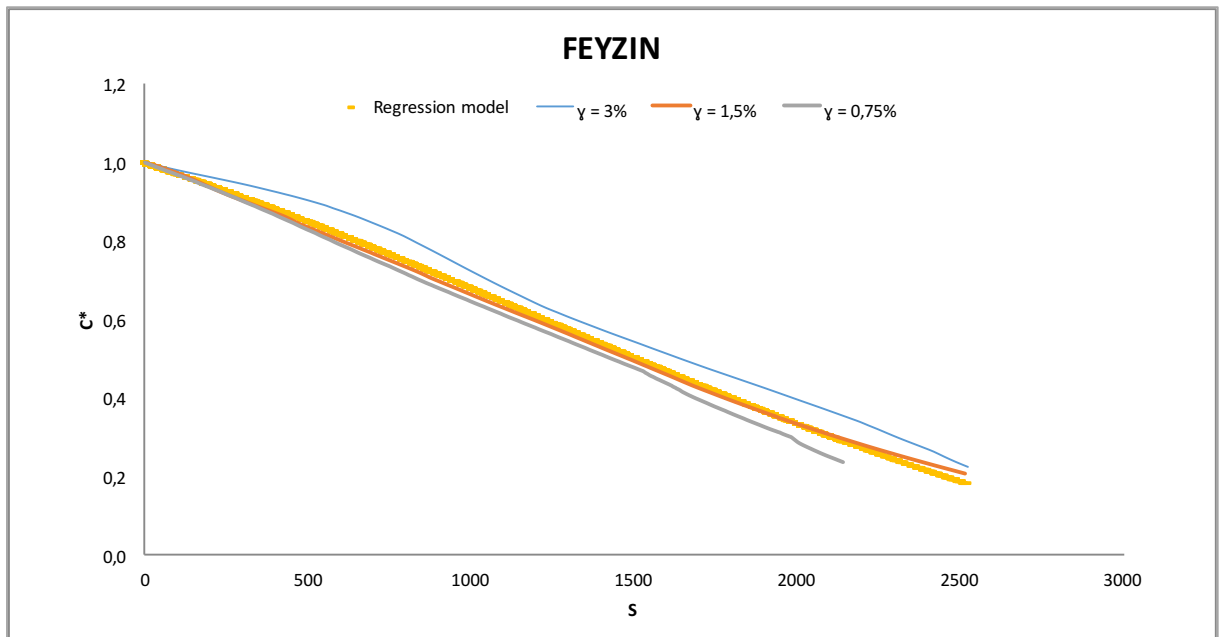
Fig. 28
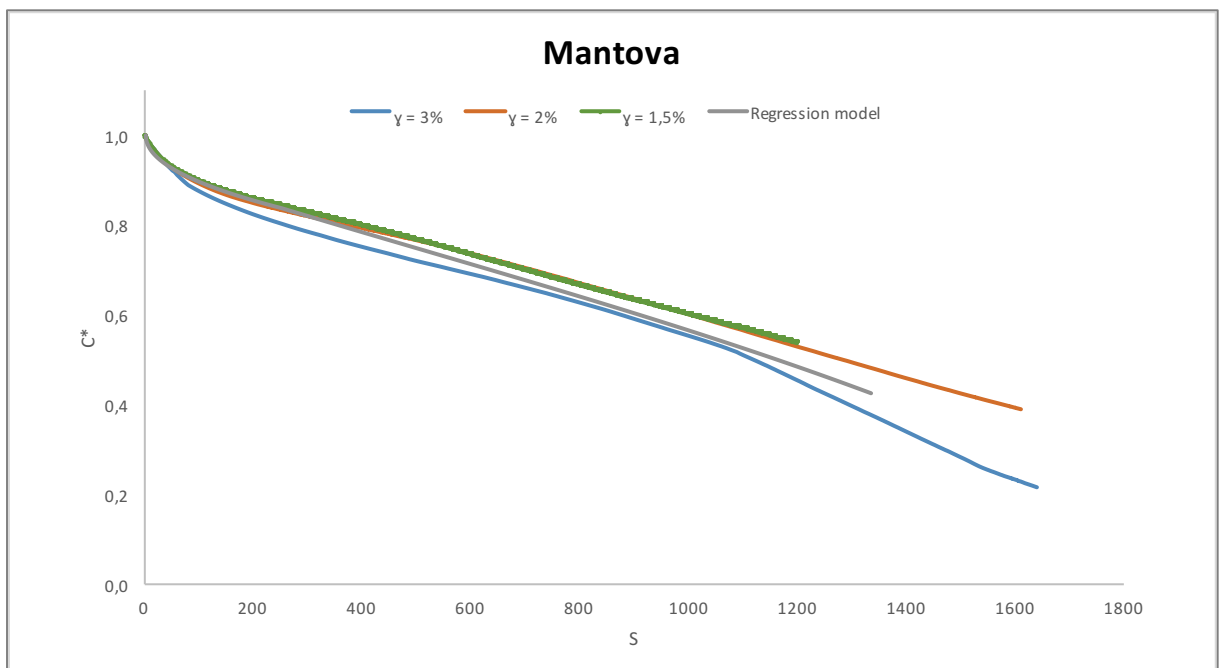
Fig. 29

In the case of Mantova (fig. 29), the tests performed at 2% and 1,5% didn't reach the 90% reduction (section 2.7) due to the fact that they take too long to be performed in one day. It's important to point out that it wasn't possible to leave the rheometer working during nighttime and therefore the tests were interrupted before they finished.

The regression model finishes at a C^* value equal to the mean of the last points of the three tests performed at different strain levels.
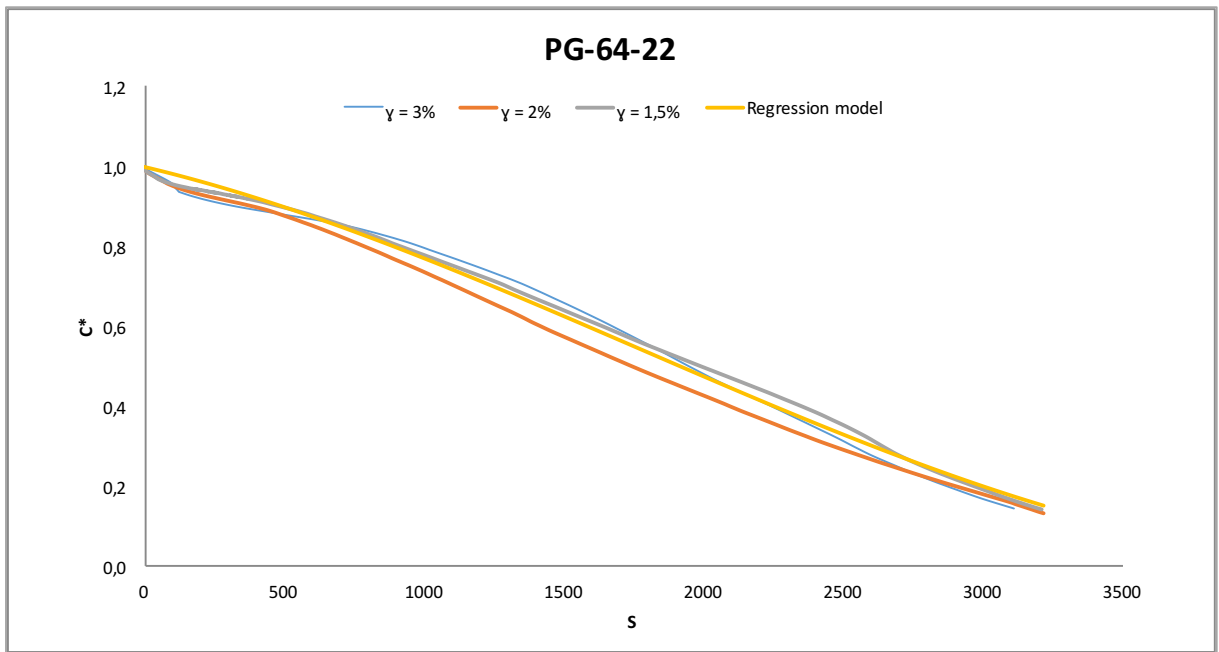
Fig. 30
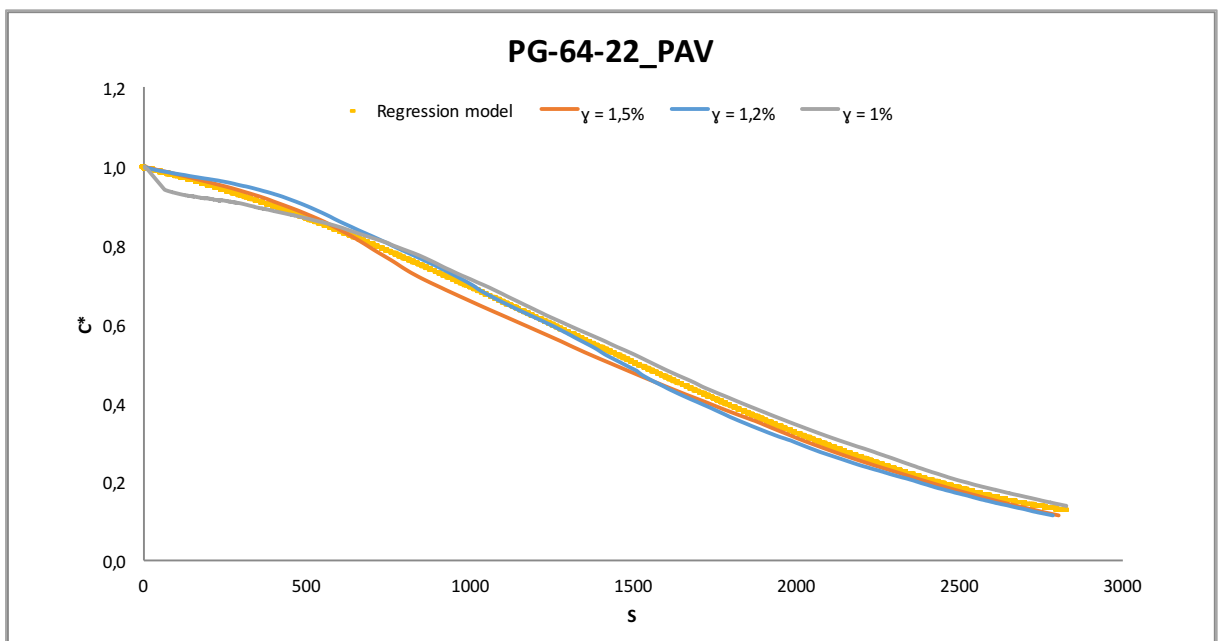
Fig. 31
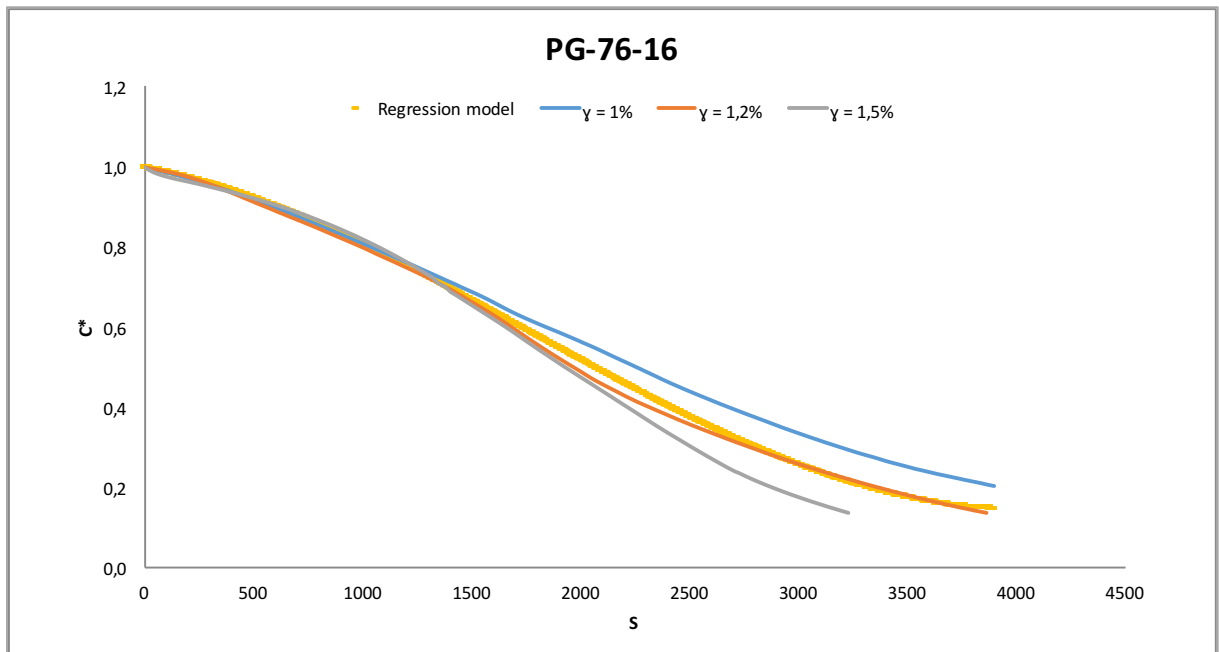
Fig. 32
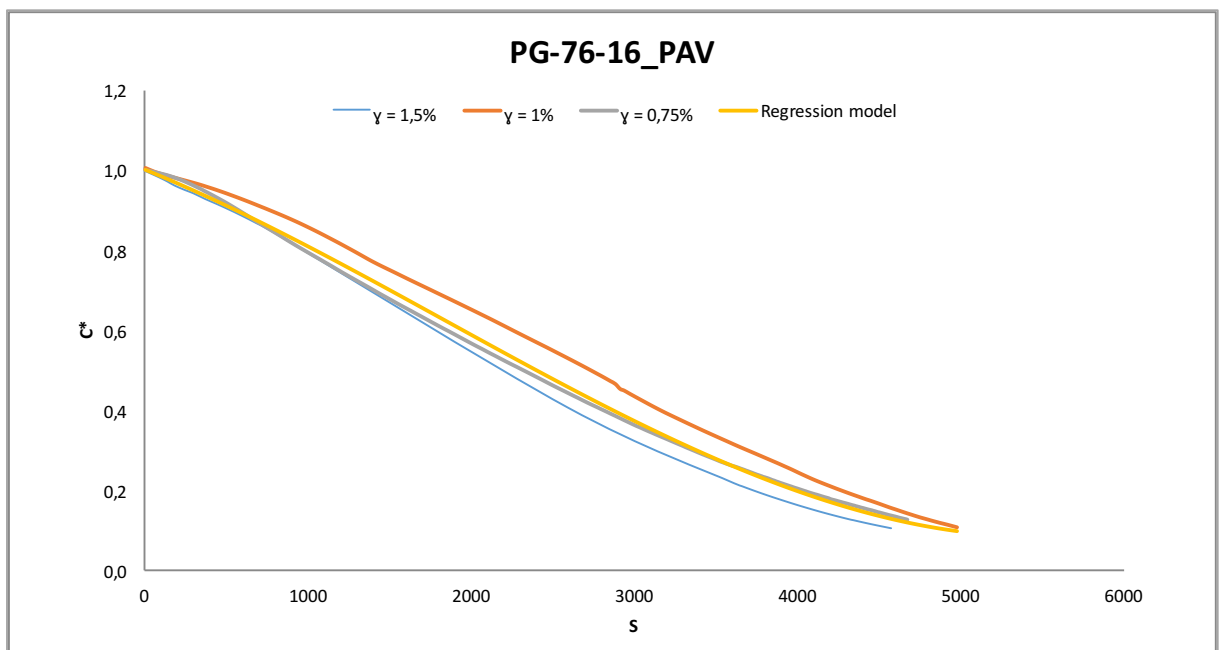
Fig. 33

In the following figure (fig. 34), it's possible to compare the regression models of the different binders studied in this work.

It's important to point out that for an equivalent reduction of pseudo stiffness, curves on the right side of the graph are able to support more damage than curves located on the left side. In other words, for an equal level of integrity a binder which curve is on the right side of another one stands more damage.

In this case, the binder with the best behavior regarding damage is the PG-76-16_PAV and the worst one is Mantova.

As explained before, the Mantova curve in fig 34 is shorter that the other ones because of time limitations regarding the time sweep tests.

Damage characteristic curves regression models

Legend: PG-76-16_PAV, PG-76-16_ORIGINAL, PG-64-22_ORIGINAL, PG-64-22_PAV, FEYZIN, MANTOVA

Fig. 34

Conclusion

This study was carried out on different asphalt binders in order to characterize their damage behavior taking into account non-linear effects. Damage characteristic curves were obtained by means of the proposed model employed in this experimental investigations.

Several conclusions were derived by comparing the original tested materials and the aged binders as well. The last part of the conclusion is dedicated to test suggestions and ideas for future works.

The four materials used in this work were selected in order to identify a variety of binders with very different compositions. In the following paragraph, the differences obtained are presented:

- The MANTOVA binder showed the strongest non-linear behavior in comparison to the rest of the binders, especially compared to FEYZIN. Besides, FEYZIN non-linear model was approximated with exponential functions while in all the other cases polynomial functions were used.
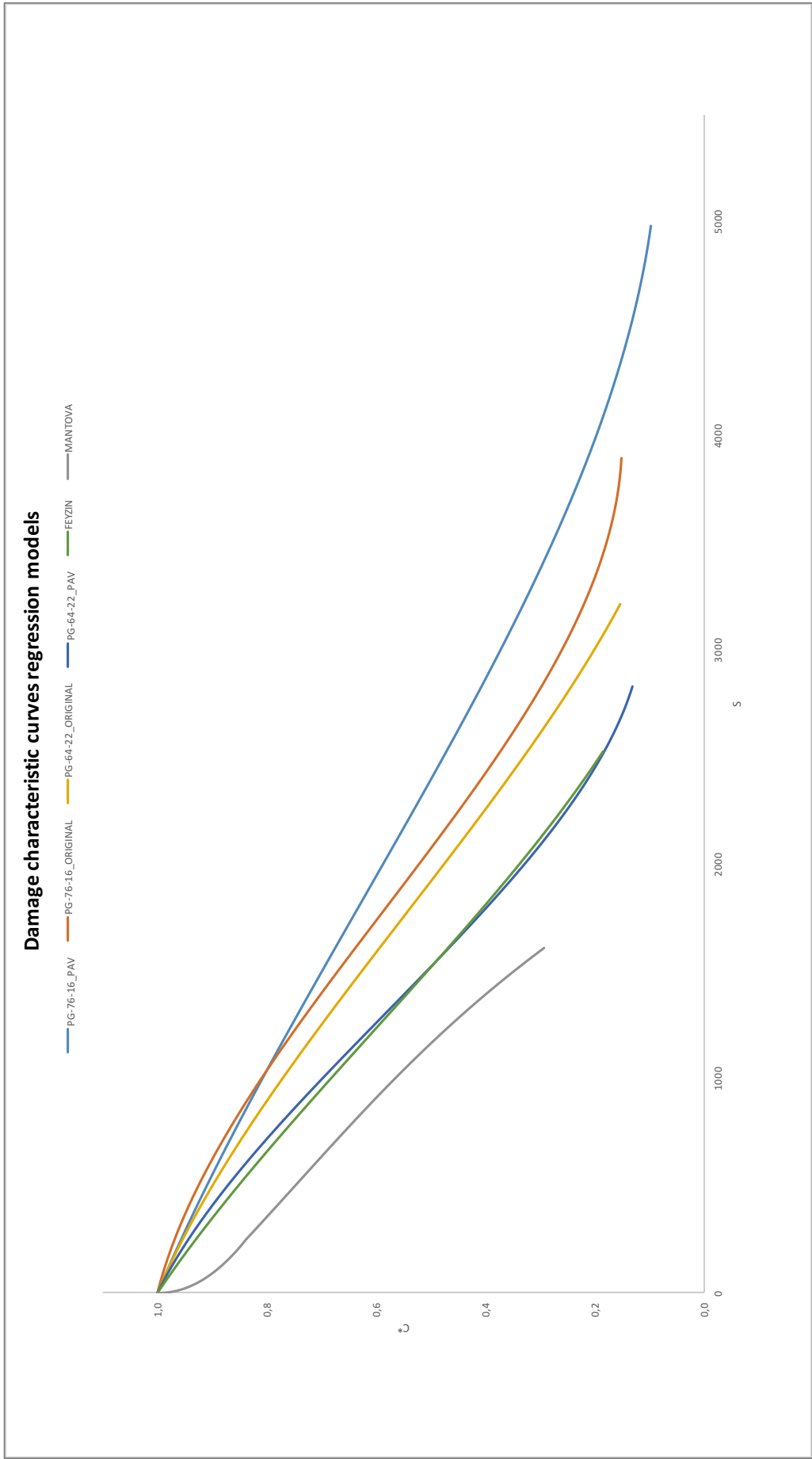- The time sweep tests performed on MANTOVA binder were the longest ones. It should be pointed out the it wasn't possible to complete some of them due to time consumption (more than one working day). On the other hand, the PG-76-16 tests were the shortest ones. It is interesting to remark that in almost all cases the time sweep tests took longer in the less rigid binders.
- MANTOVA is clearly the worst material regarding damage behavior. In fact, by considering the overall comparison of the damage characteristic curves, the MANTOVA binder endures less damage. On the contrary, the PG-76-16 binder shows the best behavior. In fact, its damage characteristic curve is the longest one. The PG-64-22 has the second best behavior in that regard.
- The shape of the MANTOVA damage characteristic curve is quite strange and different from the others. In fact, two different regression functions were needed to approximate the curve.
- By considering the complex moduli, MANTOVA is the least rigid binder while the PG-76-16 is the most rigid one.
- By comparing the PG-64-22 and the PG-76-16 binders in their original state and in their PAV state interesting conclusions were derived. Regarding the non-linear model, it was found that it is stronger in the long-term aged binders. In other words, for a certain strain, the PAV binders show a higher a_γ shift factor and a lower h_1 shift factor in comparison to the original binders.

On the basis of the experience developed during this study, some suggestions can be proposed for future works:

- It was found that one of the main hypothesis regarding the independence from strain of the damage characteristic curves was not completely respected. Indeed, in some cases, especially for FEYZIN and MANTOVA there were some differences between the curves obtained for different strain levels. Although the non-linear models provided reasonable results in most cases, the reason for this differences might be related to

the incapacity of the model to fully represent the non-linear behavior. Therefore, this might be an argument to look into in future works.

- Another interesting topic for future investigations should be represented by the relationship that might be between the colloidal index and the damage characteristic curves.

References

Findley, W. N., Lai, J. S. & Onaran, K., 1976. *Creep and Relaxation of Nonlinear Viscoelastic Materials.* 1989 a cura di New York: Dover Publications, INC.

Hou, T., Underwood, S. B. & Kim, Y. R., 2010. Fatigue Performance Prediction of North Carolina Mixtures Using the Simplified Viscoelastic Continuum Damage Model. *Journal of the Association of Asphalt Pavement Technologists,* pp. 36 - 76.

Kim, Y. R. et al., 2008. Application of Viscoelastic Continuum Damage Model Based Finite Element Analysis to Predict the Fatigue Performance of Asphalt Pavements. *KSCE Journal of Civil Engineering,* pp. 109 -120.

Marasteanu, M. & Anderson, D., 1999. Improved model for bitumen rheological characterization. *Proceedings of the Eurobitume Workshop on Performance Related Properties for Bituminous Binders,* pp. 1 - 4.

Schapery, R. A., 1984. Correspondence principles and a generalized J integral for large deformation and fracture analysis of viscoelastic media. *International Journal of Fracture,* p. 195–223.

Schapery, R. A., 1990. A theory of mechanical behavior of elastic media with growing damage and other changes in structure. *Journal of Mechanics and Physics of Solids,* p. 215–253.

Underwood, B. S., 2006. Characterization and Performance Prediction of ALF Mixtures Using a Viscoelastoplastic Continuum Damage Model. *Asphalt Paving Technolog: Association of Asphalt Paving Technologists - Proceedings of the Technical Sessions,* p. 580.

Underwood, B. S., 2012. Simplified Viscoelastic Continuum Damage Model as Platform for Asphalt Concrete Fatigue Analysis. *Transportatio Research Record,* pp. 36 - 45.

Underwood, B. S., 2015. A continuum damage model for asphalt cement and asphalt mastic fatigue. *International Journal of Fatigue,* pp. 387 - 401.

Underwood, B. S., Kim, Y. & MN, G., 2010. Improved calculation method of damage parameter in viscoelastic continuum damage model. *International Journal Pavement Eng,* pp. 459 - 476.

Underwood, B. S. & Kim, Y. R., 2014. Nonlinear viscoelastic analysis of asphalt cement and asphalt mastics. *International Journal of Pavement Engineering,* pp. 510-529.

Yun, T., Underwood, B. S. & Kim, Y. R., 2010. Time-Temperature Superposition for HMA with Growing Damage and Permanent Strain in Confined Tension and Compression. *JOURNAL OF MATERIALS IN CIVIL ENGINEERING,* pp. 415 - 422.

Zeiada, W. A. et al., 2014. Comparison of conventional, polymer, and rubber asphalt mixtures using viscoelastic continuum damage model. *Road Materials and Pavement Design,* pp. 588 - 605.

Appendix

On table 9 the experimental points obtained in the MSS tests are presented.

Binder	Reduced freq.	G* [Pa] Experimental points						
	[Hz]	γ = 0,5 %	γ = 1 %	γ = 2 %	γ = 2,5 %	γ = 3 %	γ = 4 %	γ = 5 %
FEYZIN	10,00	639.031	639.332	637.424	635.447	632.911	627.181	619.677
		639.163	638.434	635.155	632.698	628.804	623.312	615.122
	37,42	1.794.309	1.790.068	1.770.426	1.755.760	1.739.566	1.703.176	1.659.472
		1.794.153	1.789.602	1.770.848	1.756.961	1.741.638	1.707.046	1.659.472
	163,81	5.117.986	5.089.864	4.964.189	4.874.954	4.779.107	4.574.026	4.345.818
		5.119.549	5.090.722	4.965.688	4.877.186	4.782.122	4.578.445	4.351.890
	930,04	14.258.639	14.061.303	13.356.195	12.909.689	12.429.612	11.427.553	10.437.852
	6143,72	38.962.034	38.248.603	35.513.606	33.688.763	31.901.367	27.770.068	23.808.967
MANTOVA	10,00	487.848	485.027	473.271	465.043	462.381	440.356	422.958
		487.812	484.292	473.439	465.812	463.430	443.519	427.679
	41,38	1.227.562	1.209.867	1.147.936	1.108.123	1.095.601	997.532	926.754
		1.226.438	1.215.560	1.158.453	1.125.821	1.114.441	1.025.204	959.939
	191,54	3.036.835	2.988.860	2.806.554	2.701.008	2.666.761	2.398.764	2.206.863
		3.033.148	2.988.933	2.816.494	2.705.957	2.672.218	2.405.295	2.219.592
	1005,17	7.301.162	7.149.646	6.586.197	6.259.492	6.152.168	5.364.602	4.839.032
		7.298.627	7.172.614	6.668.566	6.366.136	6.267.465	5.529.415	5.030.407
	6078,16	16.740.952	16.287.268	14.699.373	13.792.004	13.495.047	11.432.846	9.935.687
		16.732.169	16.317.322	14.842.310	13.966.521	13.621.721	11.615.721	10.186.803
PG - 64 - 22 Original	10,00	867.178	866.002	860.002	855.512	850.253	838.556	824.445
		867.205	865.922	859.924	855.435	850.307	838.832	824.770
	40,55	2.286.941	2.277.940	2.236.745	2.206.740	2.174.299	2.103.472	2.022.384
		2.286.363	2.278.397	2.241.419	2.214.607	2.190.854	2.183.098	2.045.280
	184,82	5.924.225	5.879.127	5.670.561	5.526.546	5.375.986	5.060.964	4.726.346
		5.924.483	5.883.395	5.688.180	5.551.472	5.408.214	5.106.829	4.784.974
	961,81	14.762.409	14.573.538	13.778.264	13.243.217	12.705.455	11.593.290	10.474.936
		14.766.995	14.565.398	13.859.808	13.355.815	12.831.968	11.743.037	10.684.652
	5818,60	34.508.932	33.899.551	31.411.843	29.752.353	28.140.173	24.463.618	20.944.524
		34.515.043	33.872.213	31.399.789	29.767.989	28.149.675	24.575.898	21.015.607
PG - 64 - 22 PAV	10,00	3.454.505	3.426.294	3.303.282	3.218.026	3.129.571	2.942.729	2.750.372
		3.452.615	3.427.157	3.298.938	3.212.795	3.121.944	2.929.055	2.735.455
	49,68	7.432.320	7.333.747	6.919.730	6.662.625	6.391.072	5.854.419	5.348.483
		7.434.834	7.343.732	6.969.503	6.719.627	6.463.408	5.956.606	5.463.714
	265,85	14.695.521	14.379.630	13.263.106	12.602.657	11.957.477	10.649.938	9.337.226
		14.681.555	14.418.688	13.400.629	12.755.334	12.065.075	10.795.010	9.460.744
	1540,27	26.970.937	26.392.868	24.327.636	22.997.063	21.679.281	19.145.572	16.403.778
	9718,06	46.224.908	45.011.293	40.868.528	38.293.123			

Binder	Reduced freq.	G* [Pa] Experimental points						
	[Hz]	γ = 0,5 %	γ = 1 %	γ = 2 %	γ = 2,5 %	γ = 3 %	γ = 4 %	γ = 5 %
PG - 76 - 16 Original	10,00	1.768.440	1.760.189	1.727.186	1.705.183	1.672.800	1.628.175	1.567.669
		1.767.836	1.759.991	1.731.224	1.710.303	1.680.611	1.639.694	1.582.161
	43,44	4.377.063	4.347.883	4.211.708	4.114.439	3.987.642	3.812.908	3.595.676
		4.377.813	4.344.551	4.191.033	4.086.130	3.947.334	3.756.067	3.525.790
	211,38	10.606.126	10.460.836	9.928.109	9.623.001	9.188.943	8.596.289	7.898.900
		10.604.856	10.478.608	10.015.698	9.679.036	9.234.258	8.626.966	7.911.560
	1168,24	24.595.748	24.247.226	22.604.190	21.558.622	20.190.584	18.272.550	15.882.680
		24.649.781	24.223.315	22.474.801	21.408.634	20.059.299	18.167.486	15.651.332
	7451,35	53.493.241	52.193.810	47.602.488	44.657.111			
		53.468.647	52.185.766	47.741.500	44.809.201			
PG - 76 - 16 PAV	10,00	9.177.549	9.034.692	8.485.942	8.150.946	7.814.423	7.152.915	6.528.934
		9.162.779	9.012.163	8.440.733	8.100.926	7.750.066	7.142.682	6.454.032
	50,74	17.310.545	16.985.076	15.716.153	15.007.276	14.290.625	12.787.219	11.399.905
		17.310.545	16.926.872	15.710.891	14.930.884	14.166.397	12.615.383	11.123.311
	281,19	31.708.638	30.907.256	28.168.306	26.491.761	24.646.438		
		31.736.044	30.997.691	28.219.854	26.411.252	24.432.881		
	1714,51	56.012.249	54.241.407					
		56.009.596	54.364.660					
	11597,35	95.199.271	90.465.744					
		95.218.043	91.914.925					

Table 9